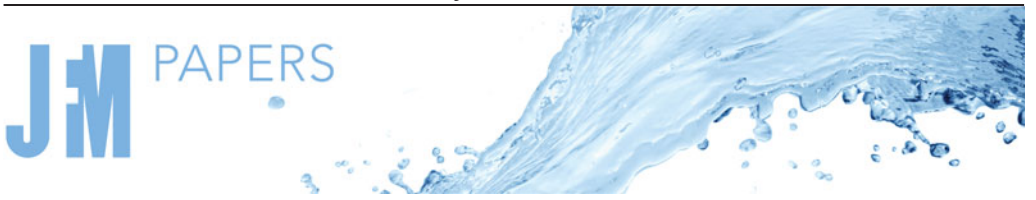
J. Fluid Mech. (2021), *vol*. 913, A40, doi:10.1017/jfm.2020.1180



Hydrodynamic forces acting on the elliptic cylinder performing high-frequency low-amplitude multi-harmonic oscillations in a viscous fluid

Artem N. Nuriev[1],†, **Andrey G. Egorov**[1] **and Ayrat M. Kamalutdinov**[1,2]

[1]Lobachevskii Institute of Mathematics and Mechanics, Kazan Federal University, 18, Kremlyovskaya St, Kazan, Tatarstan 420008, Russian Federation

[2]Department for Structural Strength, Kazan National Research Technical University named after A. N. Tupolev - KAI, 10, K.Marx St, Kazan, Tatarstan 420111, Russian Federation

(Received 1 July 2020; revised 22 December 2020; accepted 28 December 2020)

The paper is devoted to the study of the periodic rectilinear motion of an elliptic cylinder at an arbitrary angle of attack in a viscous incompressible fluid according to an arbitrary multi-harmonic law. The study develops the classical method of inner and outer asymptotic expansions of a solution in a small parameter, which is taken as the ratio of the thickness of the Stokes boundary layer to the semi-major axis of the elliptic cylinder. Another parameter of the problem, which is the Reynolds number calculated based on the thickness of the boundary layer, is considered to be of the order of unity. The selected range of values of parameters describes the low-amplitude high-frequency oscillations of the cylinder in a fluid. The asymptotic solution of the problem built in the study allows us to determine the first three terms of the expansion of the hydrodynamic force acting on the cylinder. For the detailed analysis of the obtained solution, several cases of the periodic motion of cylinders with different axis ratios for different oscillation parameters according to harmonic and multi-harmonic laws were considered. In these cases, the asymptotic dependencies of the hydrodynamic forces were compared with the data of direct numerical simulations and with known results of previous asymptotic and experimental research. The results of the analysis allow us to establish the limits of applicability of the asymptotic theory and to determine the structural changes of the hydrodynamic forces when transition to the zone of moderate oscillation amplitudes occurs.

Key words: flow–structure interactions, Navier–Stokes equations, separated flows

† Email address for correspondence: nuriev_an@mail.ru

© The Author(s), 2021. Published by Cambridge University Press

https://doi.org/10.1017/jfm.2020.1180 Published online by Cambridge University Press

1. Introduction

The first fundamental results on the interaction of oscillating bodies with a fluid were obtained in the studies of Stokes, Basset and Rayleigh in the 19th century. Since then, this area of hydrodynamics has been actively developing in different directions. Over the past two decades, there has been a significant increase of interest in the problems of interaction between oscillating elongated bodies and a fluid. Many of the studies in this direction are related to the development of innovative applied fields, such as atomic force microscopy (e.g. Sader 1998; Scherer, Frank & Gummer 2000), energy harvesting from smart materials (e.g. Aureli *et al.* 2010; Erturk & Inman 2011), cooling systems for microelectronic boards (e.g. Bidkar *et al.* 2009; Dehdari Ebrahimi, Eldredge & Ju 2019; Oh *et al.* 2019), biomimetic propulsion systems (e.g. Kopman & Porfiri 2013; Yeh & Alexeev 2014; Shintake *et al.* 2018; Yeh, Demirer & Alexeev 2019), methods for determining the properties of materials (e.g. Egorov *et al.* 2014, 2017; Paimushin, Firsov & Shishkin 2019) and fluids (e.g. Payam, Trewby & Voïtchovsky 2017) and others. The core of most modern models of interaction is the two-dimensional theory of the flow around oscillating bodies with a simple shape of the cross-sections: cylindrical, rectangular, elliptical. Even in the two-dimensional case, the determination of hydrodynamic forces acting on an oscillating body is a non-trivial task. In the zones of large and moderate amplitudes, studies of the hydrodynamics near oscillating bodies are generally based on experiments and numerical simulations. In this regard, the following studies can be noted: for a circular cylinder Keulegan & Carpenter (1958); Bearman *et al.* (1985*b*); Sarpkaya (1986); Graham & Djahansouzi (1989); Justesen (1991); An, Cheng & Zhao (2015) and Nuriev, Egorov & Zaitseva (2018), for rectangular plates Keulegan & Carpenter (1958); Shih & Buchanan (1971); Singh (1979); Graham (1980); Egorov *et al.* (2017) and Nuriev, Kamalutdinov & Egorov (2019), for a square cylinder Singh (1979) and Bearman *et al.* (1984) and for an elliptic cylinder Daoud *et al.* (2015) and Gallardo, Andersson & Pettersen (2016). In the zone of small oscillation amplitudes a complete picture of hydrodynamic processes can be obtained using asymptotic analysis.

The asymptotic theory is most well developed for the problem of the flow around a harmonically oscillating circular cylinder. The first solution of this problem for the case of infinitely small oscillation amplitudes was obtained by Stokes (1851). In the case of finite amplitude high-frequency oscillations, solutions of the problem with different orders of accuracy were obtained by Schlichting (1932), Holtsmark *et al.* (1954), Stuart (1966), Wang (1968), Riley (1967, 1975), Duck & Smith (1979), Haddon & Riley (1979), Wybrow, Yan & Riley (1996) and Nuriev & Egorov (2019).

Hydrodynamics around non-circular cylindrical bodies oscillating in a viscous fluid was also investigated in a large number of asymptotic studies, although a non-circular shape in most cases complicates the process of the analytical solution of the flow problem. The Stokes theory generalized for an arbitrary cross-section of the cylinder was formulated by Tuck (1969), however, his results give only a conceptual approach to the solution of the general problem, which formally reduced to the boundary element method. Using this method, the author obtained a semi-analytical solution of the problem of harmonic oscillations of an infinitely thin plate with an infinitely small amplitude and calculated the hydrodynamic forces acting on the plate. This method was further developed by Brumley, Willcox & Sader (2010) and Ahsan & Aureli (2015), who carried out the hydrodynamic force calculations for the problems of harmonic vibrations of plates of finite thickness and plates with flanges. It should be noted that the boundary element method gives numerical results. For practical use, according to the data of these studies, in the works of Sader (1998), Aureli & Porfiri (2010), Aureli, Porfiri & Basaran (2012), Phan, Aureli &

https://doi.org/10.1017/jfm.2020.1180 Published online by Cambridge University Press

Porfiri (2013) and Ahsan & Aureli (2015) approximate formulas for hydrodynamic forces were constructed.

Another analytical–numerical method for studying flows near square cylinders with rounding angles and cylinders with asymmetric cross-sections close to circular was considered by Kim & Troesch (1989). The authors proposed to use the Lewis transformations for the conformal mapping of the solution obtained for an oscillating circular cylinder (Riley 1967) into the desired shape. The conformal mapping allowed the first few non-stationary terms of the asymptotic expansion to be found without solving the corresponding problems, while the definition of a higher-order solution required a separate numerical calculation for each case. The obtained results describe the structural features of flows, without considering the issue of the determination of the hydrodynamic forces.

The problem of oscillations of elliptic cylinder in various approximations was investigated earlier by Ray (1936), Kanwal (1955), Davidson & Riley (1972) and Youssef (1999). Ray (1936) solved the problem in the Stokes approximation, he obtained an explicit formula for the hydrodynamic force acting on an elliptic cylinder under conditions of low-frequency harmonic oscillations with an infinitely small amplitude. Kanwal (1955) solved the problem under the assumption of arbitrary frequencies and finite oscillation amplitudes, he found the solution in the form of an infinite series of Mathieu functions. However, this solution gives only a formal expression for the hydrodynamic forces, which require extensive additional calculations to determine forces for a particular case. Davidson & Riley (1972) developed the methods proposed in Riley (1967) for the analysis of the secondary flows forming near an elliptic cylinder. The work focuses only on the investigation of secondary steady streaming without considering the issue of the determination of the hydrodynamic forces. Youssef (1999), based on the asymptotic solution of the problem performed, some calculations of the hydrodynamic forces acting on a harmonically oscillating elliptic cylinder, however, he did not derive the corresponding analytical formulas for the forces.

The objectives of this study are:

(i) to analyse the hydrodynamic forces acting on an elliptic cylinder that performs low-amplitude high-frequency oscillations according to an arbitrary periodic law;
(ii) to construct explicit formulas for the determination of hydrodynamic forces;
(iii) to test these formulas and to determine their limits of applicability.

To achieve the first two objectives, an asymptotic solution of the problem is carried out. The study develops the classical method of inner and outer asymptotic expansions of a solution in the small parameter. To calculate the hydrodynamic forces, the original approach proposed by Nuriev & Egorov (2019) is used, based on the determination of forces through the flow characteristics at infinity. This approach allows us to find an analytical expression for the first three terms of the expansion of the hydrodynamic force without finding the complete solutions of the external and internal problems for high-order terms. To achieve the third objective, we consider the behaviour of the obtained formulas for a wide range of parameters and compare it with the previously known data and new results of numerical simulations that are carried out in this work.

The paper is organized as follows. In § 2 the mathematical formulation of the problem is given and the method of hydrodynamic force calculation based on the flow characteristics at infinity is presented. In § 3, the asymptotic solution of the problem is described and the analytical expressions for the hydrodynamic forces are determined. In § 4 the asymptotic results are compared with numerical and experimental data, and the structural changes

https://doi.org/10.1017/jfm.2020.1180 Published online by Cambridge University Press

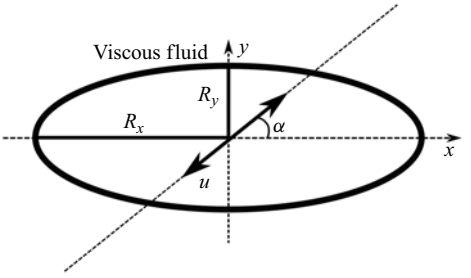


Figure 1. Scheme of the motion.

of the hydrodynamic forces appearing in the range of moderate oscillation amplitude are analysed. Concluding remarks on the work are given in § 5.

2. Mathematical formulation of the problem

2.1. *Governing equations*

Consider a fluid flow around an elliptic cylinder with semi-axes R_x and R_y ($R_x \geqslant R_y$) performing high-frequency low-amplitude periodic oscillations along a straight line at an angle α to the major semi-axis (see figure 1) with velocity

$$\boldsymbol{u}(t) = (u_x(t), u_y(t)) = U_0\tilde{u}(t)(\cos\alpha, \sin\alpha), \quad \tilde{u}(t) = \mathrm{Re}\left(\sum_{k=1}^{\infty} \tilde{u}_k\, \mathrm{e}^{\mathrm{i}k\omega\tilde{t}}\right). \tag{2.1a,b}$$

Here, ω determines the oscillation period $T = 2\pi/\omega$, whereas U_0 determines the characteristic amplitude of velocity oscillations. We choose U_0 so that the dimensionless velocities $\tilde{u}_k$ satisfy the condition

$$\sum_{k=1}^{\infty} k^{-1}\,|\tilde{u}_k|^2 = 1. \tag{2.2}$$

It is convenient to study the flow in the moving elliptic coordinate system (r, θ) associated with the cylinder. The coordinates r and θ are related to the Cartesian coordinates x and y as follows:

$$x = \lambda\cosh r\cos\theta, \quad y = \lambda\sinh r\sin\theta. \tag{2.3a,b}$$

Normalizing the spatial coordinates, time and velocity by R_x, ω^{-1}, U_0 respectively, we can write the dimensionless Navier–Stokes equation (assuming incompressible flow and neglecting body forces) in terms of streamfunction ψ as

$$\frac{\partial}{\partial t}\Delta\psi + \frac{\gamma\varepsilon}{\lambda^2 h^2}\frac{\partial(\psi, \Delta\psi)}{\partial(r, \theta)} - \varepsilon^2\Delta^2\psi = 0, \tag{2.4}$$

$$\frac{\partial\,(\psi, \Delta\psi)}{\partial\,(r, \theta)} = \left[\frac{\partial\psi}{\partial r}\frac{\partial\Delta\psi}{\partial\theta} - \frac{\partial\psi}{\partial\theta}\frac{\partial\Delta\psi}{\partial r}\right], \quad h = \sqrt{\cosh^2 r - \cos^2\theta}, \quad \lambda = \sqrt{1 - b^2}, \tag{2.5a–c}$$

where Δ is the Laplace operator. The dimensionless parameters of the problem are defined as follows:

$$\varepsilon = \frac{d_{st}}{R_x}, \quad \gamma = \frac{U_0 d_{st}}{\nu}, \quad d_{st} = \sqrt{\frac{\nu}{\omega}}, \quad b = R_y/R_x, \tag{2.6a–c}$$

https://doi.org/10.1017/jfm.2020.1180 Published online by Cambridge University Press

where ν is the kinematic viscosity of the fluid. The dimensionless parameter ε determines the ratio of the thickness of the Stokes unsteady boundary layer d_{st} (see Landau & Lifshitz 1987) to the length of the semi-major axis. For the case of high-frequency oscillations d_{st} is small so $\varepsilon \ll 1$. The dimensionless parameter γ is the analogue of the Reynolds number based on the thickness of the boundary layer d_{st}. Further, we assume that it takes values of the order of unity.

In a moving coordinate system on the surface of the cylinder we set no-slip boundary conditions and at infinity we set the boundary condition corresponding to an oscillating flow

$$r = r_0 = \ln\left(\frac{\sqrt{1+b}}{\sqrt{1-b}}\right) : \ \psi = \frac{\partial \psi}{\partial r} = 0, \tag{2.7}$$

$$r \to \infty : \ \psi \sim \lambda\, \mathrm{e}^{r} \sin(\theta - \alpha)\tilde{u}, \quad \tilde{u} = \mathrm{Re}\left(\sum_{k=1}^{\infty} \tilde{u}_k\, \mathrm{e}^{\mathrm{i}k\tilde{t}}\right). \tag{2.8a,b}$$

2.2. *Force calculation*

One of the most important flow characteristics is the hydrodynamic force exerted on the cylinder by the fluid (per unit length). We will calculate it through the characteristics of the flow at infinity (see, e.g. Noca, Shiels & Jeon 1999). For the considered case, the formulas for calculation of the components of the force $\boldsymbol{F} = (F_x, F_y)$ can be represented in the following form:

$$F_{x,y} = L_{x,y}(\psi) + \varepsilon N_{x,y}(\psi, \psi) + \varepsilon^2 I_{x,y}(\psi), \tag{2.9}$$

$$L_x(\psi) = \lambda \frac{\partial}{\partial t} \int_0^{2\pi} \left(\frac{\partial \psi}{\partial r} \sinh r - \psi \cosh r\right)\Big|_{r\to\infty} \sin\theta \, \mathrm{d}\theta, \tag{2.10}$$

$$L_y(\psi) = -\lambda \frac{\partial}{\partial t} \int_0^{2\pi} \left(\frac{\partial \psi}{\partial r} \cosh r - \psi \sinh r\right)\Big|_{r\to\infty} \cos\theta \, \mathrm{d}\theta, \tag{2.11}$$

$$\begin{aligned} N_x(\psi, \psi) = {} & -\gamma\lambda \int_0^{2\pi} \left(\frac{\partial \psi}{\partial \theta} \sinh r \Delta\psi\right)\Big|_{r\to\infty} \sin\theta \, \mathrm{d}\theta \\ & - \gamma \int_0^{2\pi} \left(\frac{1}{2} \frac{\sinh r \cos\theta}{\lambda h^2} \left(\left(\frac{\partial \psi}{\partial r}\frac{\partial \psi}{\partial r}\right) - \left(\frac{\partial \psi}{\partial \theta}\frac{\partial \psi}{\partial \theta}\right)\right)\right. \\ & \left. - \frac{\sin\theta \cosh r}{\lambda h^2} \frac{\partial \psi}{\partial \theta}\frac{\partial \psi}{\partial r}\right)\Big|_{r\to\infty} \mathrm{d}\theta, \end{aligned} \tag{2.12}$$

$$\begin{aligned} N_y(\psi, \psi) = {} & \gamma\lambda \int_0^{2\pi} \left(\frac{\partial \psi}{\partial \theta} \cosh r \Delta\psi\right)\Big|_{r\to\infty} \cos\theta \, \mathrm{d}\theta \\ & - \gamma \int_0^{2\pi} \left(\frac{1}{2} \frac{\cosh r \sin\theta}{\lambda h^2} \left(\left(\frac{\partial \psi}{\partial r}\frac{\partial \psi}{\partial r}\right) - \left(\frac{\partial \psi}{\partial \theta}\frac{\partial \psi}{\partial \theta}\right)\right)\right. \\ & \left. + \frac{\cos\theta \sinh r}{\lambda h^2} \frac{\partial \psi}{\partial \theta}\frac{\partial \psi}{\partial r}\right)\Big|_{r\to\infty} \mathrm{d}\theta. \end{aligned} \tag{2.13}$$

The last term in (2.9) vanishes at infinity.

https://doi.org/10.1017/jfm.2020.1180 Published online by Cambridge University Press

The force $\boldsymbol{F}$ acting on the cylinder in the oscillatory flow differs from the force $\boldsymbol{F}^*$ acting on the oscillating cylinder in the still fluid by the Froude–Krylov force $\boldsymbol{F}^f$

$$\boldsymbol{F} = \boldsymbol{F}^* + \boldsymbol{F}^f. \tag{2.14}$$

For the present case, $\boldsymbol{F}^f = (F_x^f, F_y^f)$ can be calculated as

$$F_x^f = \frac{\partial \tilde{u}}{\partial t} \cos\alpha \int_0^{2\pi} \cos^2\theta \sqrt{\frac{1-\lambda^2\cos^2\theta}{1+\lambda^2\cos^2\theta}}\, \mathrm{d}\theta, \tag{2.15}$$

$$F_y^f = b^2 \frac{\partial \tilde{u}}{\partial t} \sin\alpha \int_0^{2\pi} \sin^2\theta \sqrt{\frac{1-\lambda^2\cos^2\theta}{1+\lambda^2\cos^2\theta}}\, \mathrm{d}\theta. \tag{2.16}$$

Note that, in accordance with the normalization used, all the determined components of the force are non-dimensionalized by $F_0 = \rho R_x^2 U_0 \omega$.

3. Asymptotic solution

3.1. *Asymptotic expansions*

The solution of the problem (2.4)–(2.8*a*,*b*) consists of oscillatory $\tilde{\psi}$ and steady $\bar{\psi}$ parts

$$\psi = \tilde{\psi} + \bar{\psi}. \tag{3.1}$$

We separate equation (2.4) into a pair of equations describing oscillatory and stationary flows

$$\frac{\partial}{\partial t}\Delta\tilde{\psi} + \frac{\gamma\varepsilon}{\lambda^2 h^2}\left[\frac{\partial\left(\bar{\psi}, \Delta\tilde{\psi}\right)}{\partial(r,\theta)} + \frac{\partial\left(\tilde{\psi}, \Delta\bar{\psi}\right)}{\partial(r,\theta)}\right] + \frac{\gamma\varepsilon}{\lambda^2 h^2}\left[\frac{\partial\left(\tilde{\psi}, \Delta\tilde{\psi}\right)}{\partial(r,\theta)}\right]_u = \varepsilon^2 \Delta^2 \tilde{\psi}, \tag{3.2}$$

$$\frac{\gamma\varepsilon}{\lambda^2 h^2}\left[\frac{\partial\left(\bar{\psi}, \Delta\bar{\psi}\right)}{\partial(r,\theta)}\right] + \frac{\gamma\varepsilon}{\lambda^2 h^2}\left[\frac{\partial\left(\tilde{\psi}, \Delta\tilde{\psi}\right)}{\partial(r,\theta)}\right]_s = \varepsilon^2 \Delta^2 \bar{\psi}. \tag{3.3}$$

Here, subscripts u and s denote the oscillatory and the steady parts of the expression, respectively. To solve the problem we use the method of matched asymptotic expansions.

As is easy to see, the solution of the problem in the leading term (ε^0) is a harmonic function that determines the potential flow around the cylinder. Such a solution satisfies only one boundary condition on the body. From this we get that there must be a boundary layer near the cylinder. So we represent the oscillatory and steady components in the form of decompositions in the external and internal (boundary-layer) regions.

In the external region we expand the streamfunction as a power series in parameter ε

$$\left.\begin{aligned} \tilde{\psi} &= \tilde{\Psi}_0(r,\theta,t) + \varepsilon\tilde{\Psi}_1(r,\theta,t) + \varepsilon^2\tilde{\Psi}_2(r,\theta,t) + \cdots, \\ \bar{\psi} &= \varepsilon\bar{\Psi}_1(r,\theta) + \varepsilon^2\bar{\Psi}_2(r,\theta) + \cdots. \end{aligned}\right\} \tag{3.4}$$

The expansion in ε is effectively an expansion in a dimensionless frequency; the effects of finite amplitude are represented by the parameter γ.

https://doi.org/10.1017/jfm.2020.1180 Published online by Cambridge University Press

Substituting (3.4) into (3.2) and collecting terms involving the same powers of ε, we get the following sub-problems for the first three unsteady terms:

$$\Delta\tilde{\Psi}_j = 0, \quad j = 0, 1. \tag{3.5}$$

$$\frac{\partial}{\partial t}\Delta\tilde{\Psi}_2 + \frac{\gamma\varepsilon}{\lambda^2 h^2}\left[\frac{\partial\left(\tilde{\Psi}_0, \Delta\bar{\Psi}_1\right)}{\partial\left(r, \theta\right)}\right] = 0. \tag{3.6}$$

Internal expansion is constructed in the unsteady boundary layer $r - r_0 \sim \varepsilon$. Introducing the boundary-layer coordinate

$$\eta = \frac{r - r_0}{\varepsilon} \tag{3.7}$$

we can write the formal power series expansion of the boundary-layer solution in the form

$$\left.\begin{aligned}\tilde{\psi} &= \varepsilon\tilde{\psi}_0\left(\eta, \theta, t\right) + \varepsilon^2\tilde{\psi}_1\left(\eta, \theta, t\right) + \varepsilon^3\tilde{\psi}_2\left(\eta, \theta, t\right) + \cdots, \\ \bar{\psi} &= \varepsilon^2\bar{\psi}_1\left(\eta, \theta\right) + \varepsilon^3\bar{\psi}_2\left(\eta, \theta\right) + \cdots.\end{aligned}\right\} \tag{3.8}$$

We rewrite (3.2) in the boundary-layer coordinate system (η, θ), taking into account that

$$\left.\begin{aligned}\lambda^{-2}h^{-2} &= a_1 - a_2\varepsilon + \cdots = h_0^{-2} - \lambda^2 h_0^{-4} 2\eta\cosh r_0 \sinh r_0\varepsilon + \cdots, \\ h_0 &= \lambda\sqrt{\left(\cosh^2 r_0 - \cos^2\theta\right)}.\end{aligned}\right\} \tag{3.9}$$

Substituting (3.8) into the resulting equation and collecting terms involving the same powers of ε, we get a number of boundary-layer sub-problems. For the first two unsteady terms we have

$$\frac{\partial}{\partial t}\frac{\partial^2\tilde{\psi}_0}{\partial\eta^2} - a_1\frac{\partial^4\tilde{\psi}_0}{\partial\eta^4} = 0, \tag{3.10}$$

$$\frac{\partial}{\partial t}\frac{\partial^2\tilde{\psi}_1}{\partial\eta^2} - a_1\frac{\partial^4\tilde{\psi}_1}{\partial\eta^4} = -\gamma\left[\frac{\partial\left(\tilde{\psi}_0, a_1\dfrac{\partial^2\tilde{\psi}_0}{\partial\eta^2}\right)}{\partial\left(\eta, \theta\right)}\right]_u - \frac{\partial}{\partial\eta^2}a_2\frac{\partial^2\tilde{\psi}_0}{\partial\eta^2}. \tag{3.11}$$

The priority in solving the sub-problems is determined by the matching conditions. For functions $\tilde{\psi}_j$ they can be written as follows:

$$\left.\begin{aligned}\tilde{\psi}_0\Big|_{\eta\to\infty} &\sim \tilde{\Psi}_1\Big|_{r\to r_0} + \eta\frac{\partial\tilde{\Psi}_0}{\partial r}\bigg|_{r\to r_0}, \\ \tilde{\psi}_1\Big|_{\eta\to\infty} &\sim \tilde{\Psi}_2\Big|_{r\to r_0} + \eta\frac{\partial\tilde{\Psi}_1}{\partial r}\bigg|_{r\to r_0} + \frac{\eta^2}{2}\frac{\partial^2\tilde{\Psi}_0}{\partial r^2}\bigg|_{r\to r_0}.\end{aligned}\right\} \tag{3.12}$$

The resulting asymptotic expansion scheme is shown in figure 2.

https://doi.org/10.1017/jfm.2020.1180 Published online by Cambridge University Press

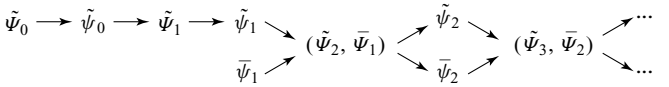


Figure 2. Asymptotic expansion scheme.

Hydrodynamic forces acting on a cylinder can be represented as a power series in parameter ε

$$\boldsymbol{F} = \boldsymbol{f}_0 + \varepsilon \boldsymbol{f}_1 + \varepsilon^2 \boldsymbol{f}_2 + \cdots, \tag{3.13}$$

where coefficients $\boldsymbol{f}_j$ are calculated by the formulas

$$\left.\begin{gathered} \boldsymbol{f}_0 = \boldsymbol{L}\left(\tilde{\Psi}_0\right), \quad \boldsymbol{f}_1 = \boldsymbol{L}\left(\tilde{\Psi}_1\right) + \boldsymbol{N}\left(\tilde{\Psi}_0, \tilde{\Psi}_0\right) \\ \boldsymbol{f}_2 = \boldsymbol{L}\left(\tilde{\Psi}_2\right) + \boldsymbol{N}\left(\tilde{\Psi}_1, \tilde{\Psi}_0\right) + \boldsymbol{N}\left(\tilde{\Psi}_0, \tilde{\Psi}_1\right) + \boldsymbol{N}\left(\bar{\Psi}_1, \tilde{\Psi}_0\right) + \boldsymbol{N}\left(\tilde{\Psi}_0, \bar{\Psi}_1\right) + \boldsymbol{I}(\tilde{\Psi}_0). \end{gathered}\right\} \tag{3.14a–c}$$

3.2. *Determination of* $\tilde{\Psi}_0$

The external solution (3.15*a*,*b*) in the leading term is determined from the equation (3.5) with the condition (2.8*a*,*b*) at infinity and the no-penetration condition for $r = r_0$ (see, e.g. Milne-Thomson 1960)

$$\tilde{\Psi}_0 = \tilde{u}(t) S(r, \theta), \quad S(r, \theta) = \lambda \, \mathrm{e}^{r_0} \sinh(r - r_0) \sin(\theta - \alpha). \tag{3.15a,b}$$

It describes the potential flow of an ideal fluid around a cylinder.

The force component $\boldsymbol{f}_0 = (f_{x,0}, f_{y,0})$ corresponding to the leading term

$$f_{x,0} = \frac{\mathrm{d}\tilde{u}(t)}{\mathrm{d}t} \lambda^2 \pi \, \mathrm{e}^{r_0} \sinh r_0 \cos\alpha = \frac{\mathrm{d}\tilde{u}(t)}{\mathrm{d}t} b(1+b)\pi \cos\alpha, \tag{3.16}$$

$$f_{y,0} = \frac{\mathrm{d}\tilde{u}(t)}{\mathrm{d}t} \lambda^2 \pi \, \mathrm{e}^{r_0} \cosh r_0 \sin\alpha = \frac{\mathrm{d}\tilde{u}(t)}{\mathrm{d}t} (1+b)\pi \sin\alpha \tag{3.17}$$

describes added mass force.

3.3. *Determination of* $\tilde{\psi}_0$

The solution of the internal sub-problem (3.10) (for determination of $\tilde{\psi}_0$) with boundary conditions

$$\tilde{\psi}_0\Big|_{\eta=0} = 0, \quad \left.\frac{\partial \tilde{\psi}_0}{\partial \eta}\right|_{\eta=0} = 0, \quad \tilde{\psi}_0\Big|_{\eta\to\infty} \sim \eta \left.\frac{\partial \tilde{\Psi}_0}{\partial r}\right|_{r\to r_0} = \eta \tilde{u}(t) \lambda \, \mathrm{e}^{r_0} \sin(\theta - \alpha), \tag{3.18a–c}$$

can be written as

$$\tilde{\psi}_0 = \lambda \, \mathrm{e}^{r_0} \frac{\sin(\theta - \alpha)}{h_0} \operatorname{Re}\left(\sum_{k=1}^{\infty} \tilde{u}_k \, \mathrm{e}^{\mathrm{i}kt} \left(\eta h_0 + \frac{1}{\sqrt{\mathrm{i}k}}\left(\exp(-\sqrt{\mathrm{i}k}\eta h_0) - 1\right)\right)\right). \tag{3.19}$$

For $\eta \to \infty$ we get

$$\eta \to \infty: \ \tilde{\psi}_0 = \eta \tilde{u}(t) \lambda \, \mathrm{e}^{r_0} \sin(\theta - \alpha) - \lambda \, \mathrm{e}^{r_0} \frac{\sin(\theta - \alpha)}{h_0} \frac{\mathrm{d}^{1/2}\tilde{x}}{\mathrm{d}t^{1/2}} + \exp. \tag{3.20}$$

https://doi.org/10.1017/jfm.2020.1180 Published online by Cambridge University Press

Here and below, 'exp' denotes exponentially small terms. The fractional derivative of the function $\tilde{x}$ describing the movement of the cylinder ($\tilde{u} = \mathrm{d}\tilde{x}/\mathrm{d}t$) is defined as

$$\frac{\mathrm{d}^{1/2}\tilde{x}}{\mathrm{d}t^{1/2}} = \mathrm{Re}\left(\sum_{k=1}^{\infty} \tilde{x}_k \sqrt{\mathrm{i}k}\, \mathrm{e}^{\mathrm{i}kt}\right) = \mathrm{Re}\left(\sum_{k=1}^{\infty} \frac{\tilde{u}_k}{\sqrt{\mathrm{i}k}}\, \mathrm{e}^{\mathrm{i}kt}\right). \tag{3.21}$$

3.4. *Determination of* $\tilde{\Psi}_1$

We build the solution $\tilde{\Psi}_1$ as a harmonic function satisfying equation (3.5) with the boundary conditions

$$r = 1: \ \tilde{\Psi}_1 = -\lambda\, \mathrm{e}^{r_0} \frac{\sin(\theta - \alpha)}{h_0(\theta)} \frac{\mathrm{d}^{1/2}\tilde{x}}{\mathrm{d}t^{1/2}}; \quad r \to \infty: \ \tilde{\Psi}_1 = O(1). \tag{3.22a,b}$$

The first of them is the matching condition following from (3.12), the second is the boundary condition at infinity. The solution to the corresponding problem has the form

$$\tilde{\Psi}_1 = -\lambda\, \mathrm{e}^{r_0} \frac{\mathrm{d}^{1/2}\tilde{x}}{\mathrm{d}t^{1/2}} \left(\sum_{j=1}^{\infty} \left(A_j \cos\alpha \sin(j\theta) - B_j \sin\alpha \cos(j\theta)\right) \mathrm{e}^{-j(r-r_0)}\right), \tag{3.23}$$

$$A_j = \frac{1}{\pi} \int_{-\pi}^{\pi} \frac{\sin\theta \sin(j\theta)}{\lambda\sqrt{\cosh^2 r_0 - \cos^2\theta}}\, \mathrm{d}\theta, \quad B_j = \frac{1}{\pi} \int_{-\pi}^{\pi} \frac{\cos\theta \cos(j\theta)}{\lambda\sqrt{\cosh^2 r_0 - \cos^2\theta}}\, \mathrm{d}\theta. \tag{3.24a,b}$$

This solution allows us to calculate the next component of the force using formula (3.14*a–c*). Since $N_{x,y}(\tilde{\Psi}_0, \tilde{\Psi}_0) = 0$, we have

$$f_{x,1} = L_x(\tilde{\Psi}_1) = \lambda^2\, \mathrm{e}^{2r_0} \pi \cos\alpha A_1 \frac{\mathrm{d}}{\mathrm{d}t} \frac{\mathrm{d}^{1/2}\tilde{x}}{\mathrm{d}t^{1/2}} = (1+b)^2 \pi \cos\alpha A_1 \frac{\mathrm{d}^{1/2}\tilde{u}}{\mathrm{d}t^{1/2}}$$
$$= (1+b)^2 \sqrt{\pi} \cos\alpha A_1 \int_{-\infty}^{t} \frac{\mathrm{d}\tilde{u}}{\mathrm{d}\tau} \frac{\mathrm{d}\tau}{\sqrt{t-\tau}}, \tag{3.25}$$

$$f_{y,1} = (1+b)^2 \sqrt{\pi} \sin\alpha B_1 \int_{-\infty}^{t} \frac{\mathrm{d}\tilde{u}}{\mathrm{d}\tau} \frac{\mathrm{d}\tau}{\sqrt{t-\tau}}. \tag{3.26}$$

Thus, $\boldsymbol{f}_1$ represents the history force (Basset force) in its classical form.

The integrals A_1, B_1 can be calculated analytically in two limiting cases:

(i) for the case of a circular cylinder ($b = 1$)

$$A_1 = B_1 = 1; \tag{3.27}$$

(ii) for the case of an infinite thin plate ($b = 0$)

$$A_1 = 4/\pi \tag{3.28}$$

and the integral B_1 diverges, i.e. it is possible to estimate the hydrodynamic force only for the angles of attack $\alpha = 0, \pi$.

https://doi.org/10.1017/jfm.2020.1180 Published online by Cambridge University Press

For the remaining cases, the values of the integrals can be found numerically. The numerical data in the range $0.05 < b < 1$ are well approximated by the following formulas:

$$A_1 \approx \frac{3.811b + 0.8749}{b^2 + 3b + 0.6874}, \quad B_1 \approx \frac{1.357b + 0.1067}{b^2 + 0.4472b + 0.01562}. \tag{3.29a,b}$$

The maximum difference between these approximations and the exact values of the integrals does not exceed 0.04 %.

3.5. *Determination of* $\tilde{\psi}_1$

The component $\tilde{\psi}_1$ can be found from the solution of the problem (3.11) with boundary conditions

$$\left.\begin{aligned} \tilde{\psi}_1\Big|_{\eta=0} &= \left.\frac{\partial\tilde{\psi}_1}{\partial\eta}\right|_{\eta=0} = 0, \\ \tilde{\psi}_1\Big|_{\eta\to\infty} &\sim \eta\left.\frac{\partial\tilde{\Psi}_1}{\partial r}\right|_{r\to r_0} + \frac{\eta^2}{2}\left.\frac{\partial^2\tilde{\Psi}_0}{\partial r^2}\right|_{r\to r_0} \\ &= \eta\lambda\,\mathrm{e}^{r_0}\frac{\mathrm{d}^{1/2}\tilde{x}}{\mathrm{d}t^{1/2}}\left(\sum_{j=1}^{\infty} j\left(A_j\cos\alpha\,\sin(j\theta) - B_j\sin\alpha\,\cos(j\theta)\right)\right). \end{aligned}\right\} \tag{3.30}$$

The last condition here is a matching condition (see (3.12)).

Due to the linearity of the problem (3.11), (3.30), its solution can be represented as the sum of two terms

$$\tilde{\psi}_1 = \tilde{\psi}_1^{(1)} + \tilde{\psi}_1^{(2)}. \tag{3.31}$$

The first term is the solution of (3.11) with the first term (proportional to γ) on the right-hand side and zero boundary conditions. The second term is the solution of (3.11) with the second term on the right-hand side and boundary conditions (3.30).

For $\tilde{\psi}_1^{(2)}$ we get

$$\tilde{\psi}_1^{(2)} = \mathrm{Re}\left(\sum_{k=1}^{\infty}\tilde{u}_k k^{-1}\,\mathrm{e}^{\mathrm{i}kt}\tilde{g}_k\,(\eta,\theta)\right), \tag{3.32}$$

$$\begin{aligned} \tilde{g}_k(\eta,\theta) &= \lambda\,\mathrm{e}^{r_0}\lambda^2\cosh r_0\sinh r_0\frac{\sin(\theta-\alpha)}{2h_0^4} \\ &\quad\times\left(\left(\mathrm{i} - \frac{\eta h_0\sqrt{k}}{\sqrt{i}} - (\eta h_0\sqrt{k})^2\right)\exp(-\sqrt{\mathrm{i}k}\eta h_0) - \mathrm{i}\right) \\ &\quad+\lambda\,\mathrm{e}^{r_0}h_0^{-1}\left(\sum_{j=1}^{\infty} j\left(A_j\cos\alpha\,\sin(j\theta) - B_j\sin\alpha\,\cos(j\theta)\right)\right) \\ &\quad\times\left(\mathrm{i} + \frac{\eta h_0\sqrt{k}}{\sqrt{\mathrm{i}}} - \mathrm{i}\exp(-\sqrt{\mathrm{i}k}\eta h_0)\right). \end{aligned} \tag{3.33}$$

https://doi.org/10.1017/jfm.2020.1180 Published online by Cambridge University Press

For $\tilde{\psi}_1^{(1)}$ we obtain the following formula:

$$\tilde{\psi}_1^{(1)} = \gamma \frac{1}{h_0}\frac{\partial}{\partial\theta}\left(\frac{\sin(\theta-\alpha)}{h_0}\right)\frac{\sin(\theta-\alpha)}{h_0}\cdot\sum_{k=1}^{\infty}\mathrm{Re}\left\{\tilde{p}_k(\eta h_0)\,\mathrm{e}^{\mathrm{i}kt}\right\}. \tag{3.34}$$

We will not present here relations for the calculation of the complex-valued functions $\tilde{p}_k(\eta)$. They are very cumbersome and uninformative, since $\tilde{p}_k$ contains an infinite number of functions of η proportional to the product of the amplitudes of the time harmonics $\tilde{u}_n, \tilde{u}_m$, $n \pm m = k$. It should be noted that all functions $\tilde{p}_k(h_0\eta)$ and their first derivatives vanish at $\eta = 0$ and reach (exponentially) a constant value $\tilde{p}_k^0$ at infinity.

The behaviour of inner solution $\tilde{\psi}_1$ at infinity gives the following boundary condition for $\tilde{\Psi}_2$:

$$r = r_0:\ \tilde{\Psi}_2 = -\tilde{g}^0(\theta)\tilde{x} + \gamma\frac{1}{h_0}\frac{\partial}{\partial\theta}\left(\frac{\sin(\theta-\alpha)}{h_0}\right)\frac{\sin(\theta-\alpha)}{h_0}\sum_{k=1}^{\infty}\mathrm{Re}\left\{\tilde{p}_k^0\,\mathrm{e}^{\mathrm{i}kt}\right\}, \tag{3.35}$$

$$\tilde{g}^0(\theta) = -\lambda\,\mathrm{e}^{r_0}\lambda^2\cosh r_0\sinh r_0\frac{\sin(\theta-\alpha)}{2h_0^4} + \lambda\,\mathrm{e}^{r_0}h_0^{-1}\left(\sum_{j=1}^{\infty} j\left(A_j\cos\alpha\sin(j\theta) - B_j\sin\alpha\cos(j\theta)\right)\right). \tag{3.36}$$

3.6. *Determination of f_2*

To determine the third component of the force f_2 in the general case according to formula (3.14*a–c*) one needs to solve the sub-problems for $\bar{\Psi}_1, \tilde{\Psi}_2$. The sub-problem for $\bar{\Psi}_1$ is strongly nonlinear, so its solution (for $\gamma > 0$) can be built only numerically. At the same time, using the method proposed by Nuriev & Egorov (2019), it is possible to determine the force f_2 in projection onto the axis of oscillation (in-line component of force) using only the value of $\tilde{\Psi}_2$ at the cylinder boundary that was calculated in the previous section (see (3.35)). To obtain the corresponding formula, we multiply the equation by the function S, defined according to (3.15*a*,*b*), and integrate the result over the flow region. Finally, we get

$$\begin{aligned}&\lambda\frac{\partial}{\partial t}\int_0^{2\pi}\left(\frac{\partial\tilde{\Psi}_2}{\partial r}\,\mathrm{e}^r - \tilde{\Psi}_2\,\mathrm{e}^r\right)\Big|_{r\to\infty}\sin(\theta-\alpha)\,\mathrm{d}\theta\\ &\quad - \gamma\tilde{u}(t)\frac{\mathrm{e}^{2r_0}}{h^2}\int_0^{2\pi}\left(\Delta\bar{\Psi}_1\sinh^2(r-r_0)\right)\Big|_{r\to\infty}\sin(\theta-\alpha)\cos(\theta-\alpha)\,\mathrm{d}\theta\\ &= -\lambda\,\mathrm{e}^{r_0}\frac{\partial}{\partial t}\int_0^{2\pi}\tilde{\Psi}_2\Big|_{r\to r_0}\sin(\theta-\alpha)\,\mathrm{d}\theta.\end{aligned} \tag{3.37}$$

As can be seen, the left side of (3.37) is equal to the projection of the force f_2 vector on the oscillation axis

$$\begin{aligned}f_{\alpha,2} &= f_{x,2}\cos\alpha + f_{y,2}\sin\alpha = -\lambda\,\mathrm{e}^{r_0}\frac{\partial}{\partial t}\int_0^{2\pi}\tilde{\Psi}_2\Big|_{r\to r_0}\sin(\theta-\alpha)\,\mathrm{d}\theta\\ &= \cos\alpha\lambda\,\mathrm{e}^{r_0}\tilde{u}\int_0^{2\pi}\tilde{g}^0(\theta)\sin\theta\,\mathrm{d}\theta - \sin\alpha\lambda\,\mathrm{e}^{r_0}\tilde{u}\int_0^{2\pi}\tilde{g}^0(\theta)\cos\theta\,\mathrm{d}\theta.\end{aligned} \tag{3.38}$$

https://doi.org/10.1017/jfm.2020.1180 Published online by Cambridge University Press

Note that the $\sin\theta$, $\cos\theta$ harmonics of the function $\tilde{\Psi}_2$ at the boundary r_0 are contained only in the term $g^0(\theta)$. The final formula for $f_{\alpha,2}$ can be written as

$$f_{\alpha,2} = \tilde{u}\pi(1+b)^2\left(\cos^2\alpha\left(-\frac{1}{2}+\Sigma_A\right)+\sin^2\alpha\left(-\frac{1}{2b^2}+\Sigma_B\right)\right), \tag{3.39}$$

$$\Sigma_A = \sum_{j=1}^{\infty} j(A_j)^2, \quad \Sigma_B = \sum_{j=1}^{\infty} j(B_j)^2. \tag{3.40a,b}$$

The third component of the force is proportional to the velocity $\tilde{u}$ of motion and expresses the Stokes viscous drag. The coefficients A_j, B_j are determined by formula (3.24*a*,*b*). The corresponding series (Σ_A, Σ_B) in formula (3.39) converge for $b > 0$. In the range $0.05 < b < 1$, we can approximate their values using the following rational functions:

$$\left.\begin{aligned}\Sigma_A &\approx \frac{0.3135b^2+1.11b+0.0974}{b^2+0.4998b+0.02154},\\ \Sigma_B &\approx \frac{3.042b+0.9046}{b^3+3b^2-0.05713b+0.001518}.\end{aligned}\right\} \tag{3.41}$$

The error of the presented formulas does not exceed 0.7 %.

3.7. *The resulting formula for the in-line force*

Collecting all the expansion terms, we can obtain the following formula for the determination of the in-line force acting on the elliptic cylinder:

$$\begin{aligned} f_\alpha = {} & (1+b)\pi(b\cos^2\alpha+\sin^2\alpha)\frac{\mathrm{d}\tilde{u}(t)}{\mathrm{d}t}\\ & + \varepsilon(1+b)^2\sqrt{\pi}(A_1\cos^2\alpha+B_1\sin^2\alpha)\int_{-\infty}^{t}\frac{\mathrm{d}\tilde{u}}{\mathrm{d}\tau}\frac{\mathrm{d}\tau}{\sqrt{t-\tau}}\\ & + \varepsilon^2\pi(1+b)^2\left(\cos^2\alpha\left(-\frac{1}{2}+\Sigma_A\right)+\sin^2\alpha\left(-\frac{1}{2b^2}+\Sigma_B\right)\right)\tilde{u}+O(\varepsilon^3). \end{aligned} \tag{3.42}$$

The coefficients A_1, B_1 and Σ_A, Σ_B can be calculated directly using formulas (3.24*a*,*b*) and (3.40*a*,*b*), or using the approximations (3.29*a*,*b*) and (3.41).

To estimate the applicability range of the resulting formula (3.42) in the next section we will analyse the behaviour of the hydrodynamic forces for several special cases.

4. Limits of applicability of the asymptotic theory

4.1. *Harmonic oscillations*

Let us consider the case of harmonic oscillations when the cylinder speed is expressed in the form

$$\tilde{u} = \cos(t). \tag{4.1}$$

https://doi.org/10.1017/jfm.2020.1180 Published online by Cambridge University Press

In this case, formula (3.42) for the force calculation is rewritten as

$$f_\alpha = -(1+b)\pi(b\cos^2\alpha + \sin^2\alpha)\sin(t) + \varepsilon(1+b)^2\pi(A_1\cos^2\alpha + B_1\sin^2\alpha)\frac{\cos(t)-\sin(t)}{\sqrt{2}} + \varepsilon^2\pi(1+b)^2\left(\cos^2\alpha\left(-\frac{1}{2}+\Sigma_A\right)+\sin^2\alpha\left(-\frac{1}{2b^2}+\Sigma_B\right)\right)\cos(t)+O(\varepsilon^3). \tag{4.2}$$

Assuming $b=1$, we obtain the well-known formula for the case of a circular cylinder (see, e.g. Wang 1968)

$$f_\alpha(b=1) = -2\pi\sin(t) + \varepsilon 2\sqrt{2}\pi(\cos(t)-\sin(t)) + \varepsilon^2 2\pi\cos(t) + O(\varepsilon^3). \tag{4.3}$$

To determine the limits of applicability of the asymptotic theory, we use the numerical and experimental data available in the literature and the new numerical results obtained in this study. We conducted the numerical simulation of the flow around elliptic cylinder using the numerical model from Nuriev *et al.* (2019). The details of the simulations are described in appendix A.

The results of experimental and numerical studies (see, e.g. Shih & Buchanan 1971; Singh 1979; Bearman *et al.* 1985*a*; Sarpkaya 1986; Justesen 1991; An *et al.* 2015) of the hydrodynamic forces acting on a harmonically oscillating cylinder are usually represented in the literature as the coefficients of the Morison approximation (Morison, Johnson & Schaaf 1950). The Morison approximation is based on the representation of the total force as a sum of two components, one of which is proportional to the instantaneous acceleration of the body, the second being proportional to the square of the instantaneous velocity. In non-dimensional variables it can be written as follows:

$$f_\alpha^M = -\pi C_M \sin t + \varepsilon\gamma C_D|\cos t|\cos t. \tag{4.4}$$

As can be seen from the structure of the asymptotic formula (3.42), the force depends not only on the instantaneous characteristics of the flow but also on the history of movement. Formally, for the case of a steady flow, if we assume that $\cos t|\cos t| \approx (8/3\pi)\cos t$, then equation (3.42) can be rewritten in the representation (4.4). In this case, the history force is decomposed into two components, one of which is included in the coefficient C_M, the other being included in the coefficient C_D

$$f_\alpha \approx -\pi C_M^{(3)}\sin t + (8/3\pi)\varepsilon\gamma C_D^{(3)}\cos t, \tag{4.5}$$

$$C_M^{(3)} = (1+b)(b\cos^2\alpha+\sin^2\alpha) + \varepsilon\frac{(1+b)^2}{\sqrt{2}}(A_1\cos^2\alpha + B_1\sin^2\alpha), \tag{4.6}$$

$$C_D^{(3)} = \frac{3\pi}{8\varepsilon\gamma}\left(\varepsilon(1+b)^2\pi(A_1\cos^2\alpha+B_1\sin^2\alpha)/\sqrt{2} + \varepsilon^2\pi(1+b)^2\left(\cos^2\alpha\left(-\frac{1}{2}+\Sigma_A\right)+\sin^2\alpha\left(-\frac{1}{2b^2}+\Sigma_B\right)\right)\right). \tag{4.7}$$

Here, the superscript (i) on the coefficients $C_M^{(i)}$, $C_D^{(i)}$ indicates the order of accuracy of the asymptotic formula for the hydrodynamic force relative to the parameter ε (in this case the coefficients are defined by formula (4.2), which has an error of the order of $O(\varepsilon^3)$).

https://doi.org/10.1017/jfm.2020.1180 Published online by Cambridge University Press

The force components grouped in this way have an obvious physical interpretation: the term proportional to the velocity is the damping force (see, e.g. Landau & Lifshitz 1987) and the term proportional to the acceleration is the inertial force that affects the change of the natural frequency in the case of resonant oscillations (see, e.g. experiments of Egorov, Kamalutdinov & Nuriev 2018).

Due to the special practical importance, we also denote the relation between the non-dimensional parameters introduced in the present work (2.6*a–c*) and the classical experimental parameters that are usually used for high-amplitude harmonic oscillations as

$$\beta = \frac{(2R_x)^2\omega}{2\pi\nu} = 2/(\varepsilon^2\pi), \quad KC = 2\pi\frac{A}{2R_x} = \pi\varepsilon\gamma. \tag{4.8a,b}$$

Here KC is the Keulegan–Carpenter number, or the dimensionless oscillation amplitude, and β is the dimensionless oscillation frequency. The values of these parameters will be also presented in the text below for convenience when working with numerical and experimental data.

In figures 3 and 4 the comparison of the values of coefficients calculated by the asymptotic formulas (4.6) and various numerical and experimental data is presented. First of all, let us pay attention to the change of the coefficients C_D, C_M depending on the ratio of the semi-axes b for fixed values of the parameters $\gamma = 0.56, 1.12$, $\varepsilon = 0.056$, $\alpha = \pi/2$ ($\beta = 200$, $KC = 0.1, 0.2$). As seen in figure 3, the first two terms of the expansion describe the change of the coefficient C_M in the entire considered range $0.05 \leqslant b \leqslant 1$ with high accuracy.

The obtained asymptotic dependence for C_D does not show such a good agreement with the numerical data for all values of the parameter b. The sum of the second and third terms of the expansion ($C_D^{(3)}$) allows us to get a good approximation in the range $0.2 \leqslant b \leqslant 1$ for both $\gamma = 0.56$ and $\gamma = 1.12$. At lower values of b, when $b \sim \varepsilon$, the series in powers of ε begins to diverge. In fact, the case of the smallness of b was not taken into account when we built the expansion in the boundary layer; such an assumption requires a revision of the internal problem (3.11). At the same time, for the terms of the order $O(\varepsilon)$, the expansion remains valid. As can be seen for $\gamma = 0.56$ (and lower values) the second term of the expansion ($C_D^{(2)}$) gives a good approximation for C_D in the range $0.05 < b < 0.2$, for $\gamma = 1.12$ the difference between the numerical data and the asymptotic solution does not exceed 15 %. The deviation of the numerical data from the asymptotic solution with increasing values of γ for small values of b is associated with the reaching of the upper limit of allowable oscillation amplitudes (for a given approximation).

Let us consider the applicability limits of the obtained asymptotic theory with respect to the amplitude of oscillations. In figure 4 the graphs of changes of the hydrodynamic coefficients depending on the dimensionless amplitude (KC) are presented (in this case, the change of amplitude is proportional to the parameter γ). In addition to the asymptotic results, numerical and experimental data, the higher-order asymptotic solution for a circular cylinder (obtained by Nuriev & Egorov (2019) in the framework of the similar approximation $\varepsilon \ll 1$, $\gamma = O(1)$) is shown

$$f_\alpha(b=1) = -2\pi\sin(t) + \varepsilon 2\sqrt{2}\pi(\cos(t) - \sin(t)) + \varepsilon^2 2\pi\cos(t) + \varepsilon^3\left(-\frac{5\pi}{2\sqrt{2}}(\cos(t) + \sin(t)) + 2\pi\gamma^2\right.$$

https://doi.org/10.1017/jfm.2020.1180 Published online by Cambridge University Press

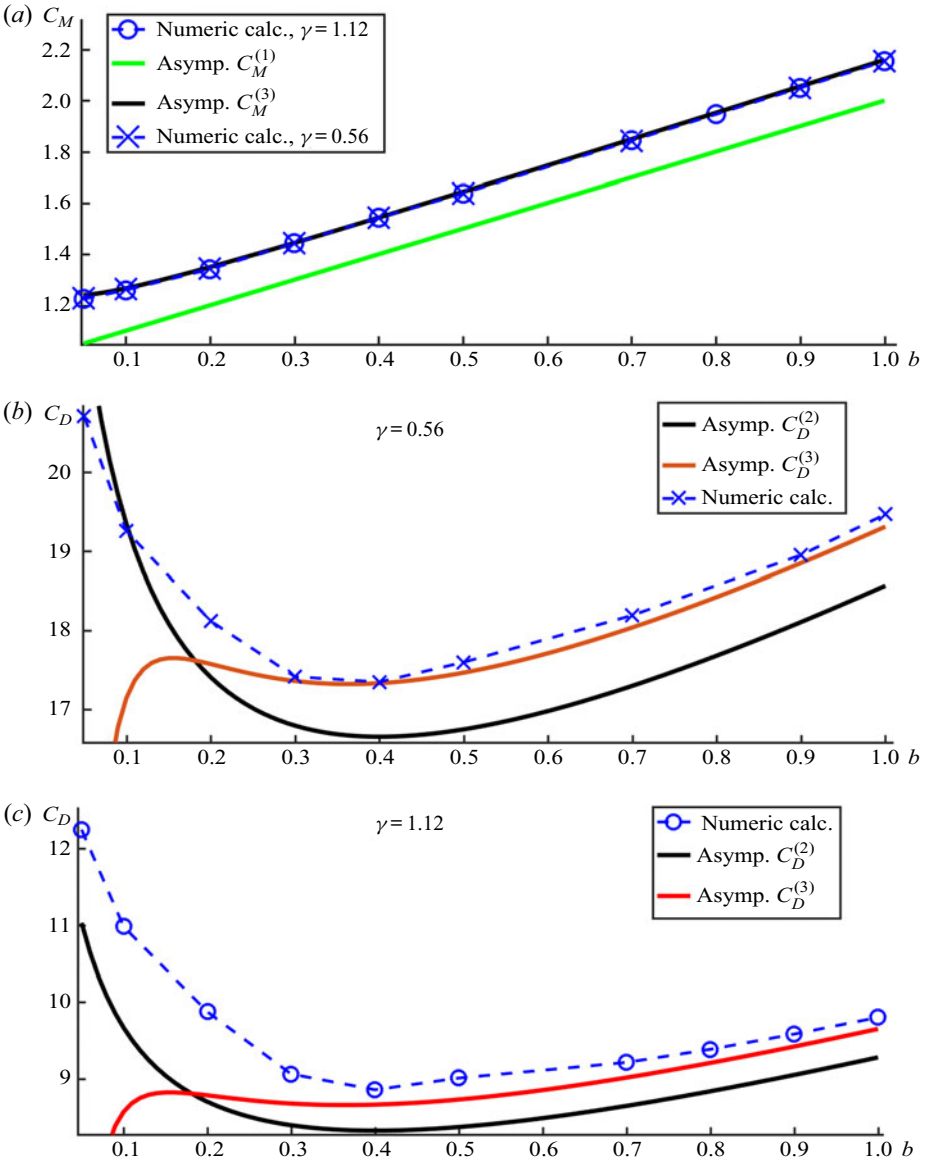


Figure 3. Harmonic oscillations. Dependences of the coefficients C_D and C_M on the parameter b. Here, $\gamma = 0.56, 1.12$, $\varepsilon = 0.056$, $\alpha = \pi/2$ ($\beta = 200$, $KC = 0.1, 0.2$)

$$\times \left(\frac{1}{3\sqrt{2}}(1 - 2\sqrt{2}) \sin(t) + \frac{5}{12}(1 + \sqrt{2}) \cos(t) \right) \Big)$$
$$+ \varepsilon^3 \gamma^2 3\pi (\sin(3t) - \cos(3t))(6\sqrt{2} + \sqrt{3} - 5 - 2\sqrt{6})/4 + O(\varepsilon^4), \quad (4.9)$$

and approximate formulas for rectangular plates obtained by Phan *et al.* (2013) for low-amplitude oscillations are presented

$$f_{plate}(b^*) \approx -\big((1.02 + 0.995b - 0.496b^2) + \varepsilon(3.07 + 1.83b - 1.245b^{0.5})\big)\pi \sin(t)$$
$$+ \big(\varepsilon(3.12 + 1.495b - 0.520b^{0.5})\big)\pi \cos(t). \quad (4.10)$$

https://doi.org/10.1017/jfm.2020.1180 Published online by Cambridge University Press

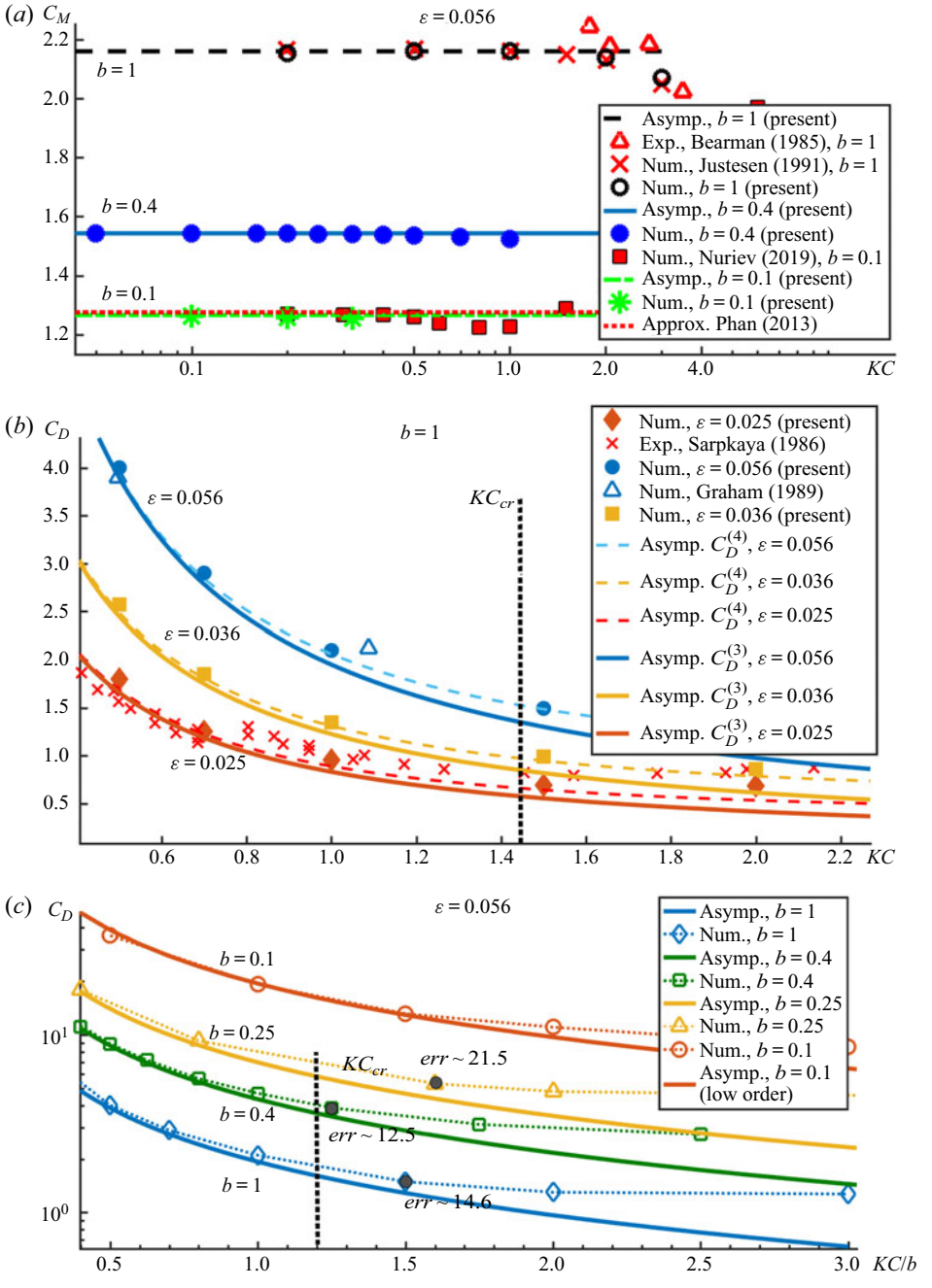


Figure 4. Harmonic oscillations. Dependences of C_D, C_M on the parameter $KC = \pi\gamma\varepsilon$ for $\alpha = \pi/2$ and different values of ε, b

The obtained theoretical estimates of the coefficient C_M coincides well with numerical data in almost the entire considered range of amplitude variation, which corresponds to symmetric flow regimes with a predominant two-dimensional structure. In addition, it can

https://doi.org/10.1017/jfm.2020.1180 Published online by Cambridge University Press

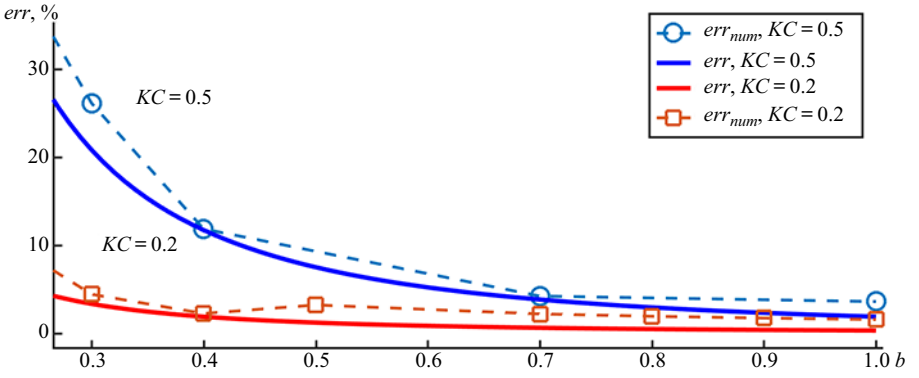


Figure 5. Harmonic oscillations. Error of the approximation $C_D^{(3)}$ as a function of the parameter b for $\varepsilon = 0.056$ ($\beta = 200$).

be noted that the values of C_M for the elliptical cylinder (4.6) and for the rectangular plate (4.10) are almost identical for small values of b ($b < 0.2$).

The theoretical formula (4.6) for C_D has more strict constraints. As can be seen, with increasing KC, the numerical data deviate from the asymptotic behaviour. For the case of $b = 1$ the deviation of the numerical data from linear theory (where the total force does not depend on γ) is well described by a nonlinear correction of the order $O(\varepsilon^3)$ that we can get from formula (4.9). The comparison of the asymptotic solution with the numerical and experimental data for this case is shown in figure 4 for $\varepsilon = 0.056, 0.036, 0.025$ ($\beta = 200, 483, 1035$). If we assume that the permissible error of the linear theory should not exceed 14 %–15 %, then we get from (4.9) the following limitation: $\gamma < \sqrt{0.21}/\varepsilon$. In this case, the critical amplitude is independent of ε and can approximately be estimated as $KC_{cr} \approx 1.44$.

Formula (4.9) also shows the presence in the hydrodynamic force of a time harmonic that is different from the main one. In other words, in addition to the damping and inertial terms, the force also contains other components. This is fully confirmed by the results of the numerical simulation. However, as can be seen, the relative contribution of these terms to the hydrodynamic force in the range of low oscillation amplitudes is small.

Based on numerical data, for cylinders with different semi-axis ratios ($b > \varepsilon$), it can be established that the limit of applicability of the asymptotic $C_D^{(3)}$ changes almost proportionally with the parameter b (for $\alpha = \pi/2$). In other words, the error of the linear theory (in per cent) can be defined as

$$err \approx 0.74 \left(\frac{KC}{b\pi}\right)^2 \times 100. \tag{4.11}$$

This can be confirmed by the comparison of the asymptotic formula for C_D with the results of numerical data for different values of $b = 1$, 0.4, 0.25 shown in figure 4, and by the direct comparison of the theoretical values of err and the values of err_{num} determined by numerical data at constant values of KC (see figure 5)

$$err_{num} = (C_D - C_D^{(3)})/C_D^{(3)} \times 100. \tag{4.12}$$

https://doi.org/10.1017/jfm.2020.1180 Published online by Cambridge University Press

For $b \sim \varepsilon$ the lower-order asymptotics $C_D^{(2)}$ works well. For the case $\varepsilon = 0.056$, $b = 0.1$ shown in figure 4, a difference of approximately 15 % between the numerical data and the asymptotic $C_D^{(2)}$ is achieved at $KC/b \approx 2$.

At the end of this section, we can also note that, although the dependences $C_D(b)$ for a plate and an elliptical cylinder have significantly different behaviour, in the range $b < 0.2$ (this can easily be seen by comparison of the corresponding asymptotic formulas in the leading terms), the values of C_D in the region of $0.05 < b < 0.2$ differ by no more than 10 %.

4.2. *Multi-harmonic oscillations*

As a second example, we consider the case when the law of the motion contains two harmonics: the first and the second. The speed of the oscillations in this case can be written in the form

$$\tilde{u} = \tilde{u}_1 \cos(t) + \tilde{u}_2 \cos(2t). \tag{4.13}$$

The asymptotic formula for determination of the force acting on the cylinder in a steady periodic flow regime for the given law of oscillations according to (3.42) is written as

$$\begin{aligned} f_\alpha = {} & -(1+b)\pi(b\cos^2\alpha + \sin^2\alpha)(\tilde{u}_1 \sin(t) + 2\tilde{u}_2 \sin(2t)) \\ & + \varepsilon(1+b)^2\pi(A_1\cos^2\alpha + B_1\sin^2\alpha)\left(\tilde{u}_1\frac{\cos(t)-\sin(t)}{\sqrt{2}} + \tilde{u}_2(\cos(2t)-\sin(2t))\right) \\ & \times \varepsilon^2\pi(1+b)^2\left(\cos^2\alpha\left(-\frac{1}{2}+\Sigma_A\right) + \sin^2\alpha\left(-\frac{1}{2b^2}+\Sigma_B\right)\right)\cdot(\tilde{u}_1\cos(t) \\ & + \tilde{u}_2\cos(2t)) + O(\varepsilon^3). \end{aligned} \tag{4.14}$$

For the analysis of the hydrodynamic force, it is again convenient to distinguish the damping and inertial components

$$f_\alpha \approx (8/3\pi)\varepsilon\gamma\sum_{k=1}^{n} C_{Dk}^{(3)} u_k \cos kt - \pi\sum_{k=1}^{n} C_{Mk}^{(3)} u_k k \sin kt, \quad n = 2, \tag{4.15}$$

$$C_{Mk}^{(3)}(\varepsilon) = C_M^{(3)}(\varepsilon/\sqrt{k}), \quad C_{Dk}^{(3)}(\varepsilon,\gamma) = C_D^{(3)}(\varepsilon/\sqrt{k}, \gamma/\sqrt{k}). \tag{4.16a,b}$$

Here, $C_{Mk}^{(3)}$ are the coefficients of the inertial forces and $C_{Dk}^{(3)}$ are the coefficients of the damping forces. Generally speaking, such a representation can also be used for an arbitrary periodic law of motion (in the approximation of the order of $O(\varepsilon^3)$), if we assume that the flow around the cylinder induced by such motion is steady. As can be seen, the coefficients $C_{Mk}^{(3)}$ and $C_{Dk}^{(3)}$ do not depend on the structure of the law of motion (for example, $C_{M1}^{(3)}$ and $C_{D1}^{(3)}$ are the same as in the case of harmonic oscillations), since interaction between different time harmonics in the found terms of expansion does not occur (it will be observed in terms of the order of $O(\varepsilon^3)$ and higher). The coefficients of the inertial forces of different time harmonics change only in the terms of the order of $O(\varepsilon)$, while the damping force of the kth harmonic increases compared to the first by $\sqrt{k}$ times (in the leading term).

Let us compare the theoretical values of the coefficients with the data from numerical simulation. The coefficients of the inertial and damping forces in the framework of

https://doi.org/10.1017/jfm.2020.1180 Published online by Cambridge University Press

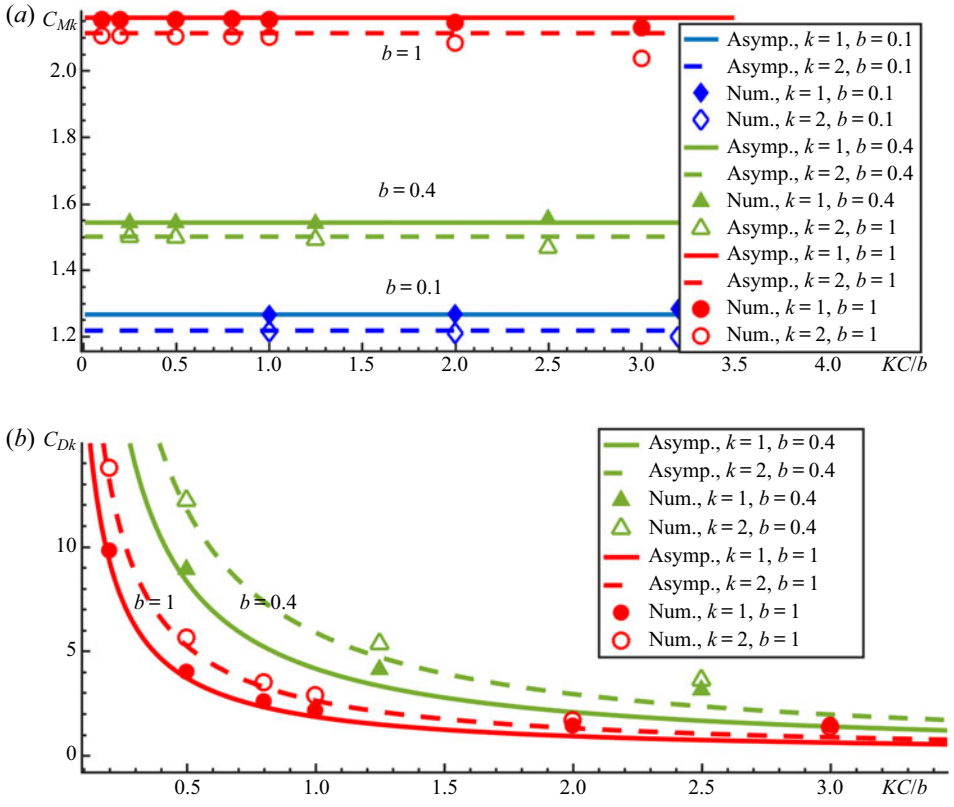


Figure 6. Multi-harmonic oscillations. Dependencies of the coefficients C_{Dk}, C_{Mk} on the dimensionless amplitude KC/b for elliptical cylinders with different semi-axis ratios at $\varepsilon = 0.056$, $\alpha = \pi/2$, ($\beta = 200$).

numerical calculations were determined using integration

$$C_{Mk} = -\frac{1}{\pi^2 u_k k}\int_{2\pi j}^{2\pi(j+1)} f_\alpha \sin kt\,\mathrm{d}t, \quad C_{Dk} = \frac{3}{8\varepsilon\gamma u_k}\int_{2\pi j}^{2\pi(j+1)} f_\alpha \cos kt\,\mathrm{d}t. \quad (4.17a,b)$$

In figure 6, the values of the coefficients for the case of $u_1 = 0.8$, $u_2 = 0.8485$, $\alpha = \pi/2$ are shown. As can be seen, the numerical values of the coefficients C_{Mk} in the studied range of $KC < 3.2$ are in good agreement with the asymptotic approximation. The numerical values of the coefficients C_{Dk}, as in the case of harmonic oscillations, begin to noticeably deviate from the theoretical values for $KC/b > 1$.

Comparing the data of multi-harmonic and harmonic oscillations, we can evaluate the influence of the new effects on the change of C_{Dk}, which arises in particular as a result of the interaction of the time harmonics. In figure 7, the deviation of the numerical data from the asymptotic (err_{num}), as well as the theoretical error estimate (err) obtained in the previous section for the case of harmonic oscillations (see formula (4.11)) are shown. As can be seen for the presented cases of multi-harmonic oscillations, the deviation of the damping force from the asymptotic for the first harmonic occurs almost 2 times faster than for the monoharmonic case, and for the second harmonic almost 4 times faster (taking into account the change of the dimensionless frequency and amplitude of the oscillations). At the same time, in the range of $KC/b < 1$ the influence of the new effects is relatively small and does not exceed 7 %–12 %. It can also be noted here that, according to the

https://doi.org/10.1017/jfm.2020.1180 Published online by Cambridge University Press

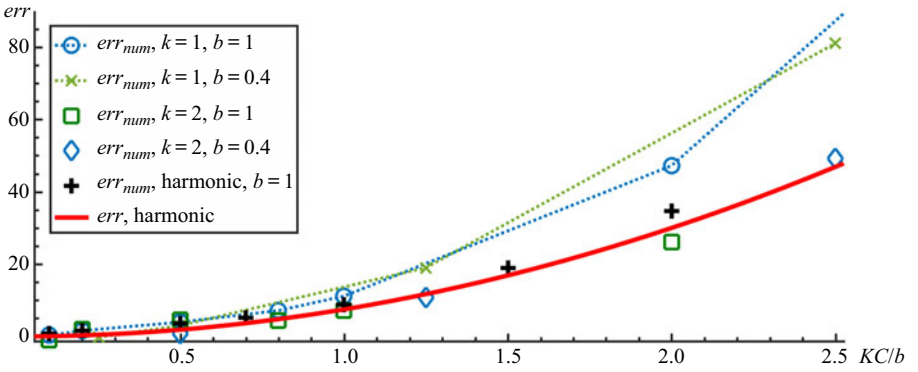


Figure 7. Multi-harmonic oscillations. The deviation of the damping force from the asymptotics depending on the dimensionless amplitude KC/b at $\varepsilon = 0.056$, $\alpha = \pi/2$, ($\beta = 200$) for elliptical cylinders with different semi-axis ratios.

numerical results for the considered case of biharmonic oscillations, with an increase of dimensionless amplitude, asymmetry of the flow regime appears (see appendix B). This leads to the appearance of a constant force component (that is an order of magnitude smaller than the damping) acting along the axis of oscillation.

5. Conclusion

The asymptotic solution of the problem constructed in the paper allows us to determine the first three terms of the expansion of the hydrodynamic force (in powers of ε) acting on an elliptic cylinder that performs low-amplitude high-frequency oscillations ($\varepsilon \ll 1$, $\gamma \sim 1$) according to an arbitrary periodic law $\boldsymbol{u}(t)$. The defined terms describe: the added mass force, proportional to $\mathrm{d}\boldsymbol{u}/\mathrm{d}t$, the history force, proportional to $\mathrm{d}^{1/2}\boldsymbol{u}/\mathrm{d}t^{1/2}$, and the Stokes resistance, proportional to $\boldsymbol{u}$ (defined along the axis of oscillation). For these force components we obtained both exact formulas for the force coefficients, expressed in terms of integrals of the functions of the parameter b, and high-precision approximations that allow us to calculate the values of the coefficients using simple explicit formulas.

In the framework of the analysis of the obtained formulas, supported by the direct numerical simulation, we studied the behaviour of the hydrodynamic forces in different cases, as well as the limitations of the asymptotic theory. Key findings can be formulated as follows:

(i) For the small oscillation amplitudes ($KC < 1$), the interaction of the time harmonics has a small effect on the hydrodynamic forces, in this case, the hydrodynamic influence on the cylinder for any multi-harmonic law of motion (in the steady periodic flow regime) can be represented as the sum of the forces acting on the cylinder oscillating with each of the harmonics forming the law. This conclusion is based on the structure of the obtained asymptotic solution and confirmed by the results of the numerical simulations.

(ii) Hydrodynamic forces acting on the cylinder performing low-amplitude oscillations under the condition of steady periodic fluid motion can be approximated with high accuracy by the sum of the inertial and damping components. From a theoretical point of view, such a representation is valid up to terms of the order of $O(\varepsilon^2)$. In the high-order terms (of the order of $O(\varepsilon^3)$ and higher), as it was shown for the

https://doi.org/10.1017/jfm.2020.1180 Published online by Cambridge University Press

case of harmonic oscillations of a round cylinder, that frequencies different from the main one appear (as a result of the interaction of the time harmonics), but their contribution at small amplitudes is insignificant.

(iii) The approximation built for the inertial forces that includes the added mass force (the term of order of $O(\varepsilon^0)$) and a part of the history force (the term of order of $O(\varepsilon^1)$) well describes the corresponding hydrodynamic effect on the cylinder in a wide range of parameters. So, in the framework of numerical modelling of harmonic and multi-harmonic oscillations, it was shown that, for the case of $\alpha = \pi/2$, the theoretical estimates are completely valid for $KC/b \leqslant 3$, and for small values of b, even in a wider range. This exceeds the expected applicability limits of the asymptotic theory.

(iv) The approximation of the damping forces, which include the second part of the history force (a term of the order of $O(\varepsilon^1)$) and the Stokes resistance (a term of the order of $O(\varepsilon^2)$), has a narrower range of applicability. A direct analysis of the structure of the obtained asymptotic formulas shows that, for small values of b, when $b \sim \varepsilon$, the series in powers of ε begins to diverge. At the same time, according to the results of the calculations, in this case ($b \sim \varepsilon$), a good approximation of the damping forces is given by the lower-order asymptotic (taking into account only the history force).

(v) The analysis of the applicability range of the asymptotics with respect to the parameter γ showed that, in the case of harmonic oscillations at $b = 1$, the fourth term of the force expansion, having the formal order of $O(\varepsilon^3)$, gives a correction proportional to $\varepsilon(KC/\pi)^2$. According to the numerical results, a similar correction proportional to $\varepsilon(KC/(b\pi))^2$ is also valid for other values of $b > \varepsilon$ (for $\alpha = \pi/2$). In other words, the error of the obtained asymptotics for the damping forces increases in proportion to the square of the dimensionless amplitude. Using the above correction, we can expand the range of applicability of the asymptotics (to $KC/b < 2$).

Funding. The reported study was supported by RSF, research project No. 19-71-00038.

Declaration of interests. The authors report no conflict of interest.

Author ORCIDs.
Artem N. Nuriev https://orcid.org/0000-0003-1561-557X.

Appendix A. Numerical simulation

For the direct numerical simulation of the flow around an elliptic cylinder we adapted the model proposed by Nuriev *et al.* (2019). The problem was solved in physical variables in a Cartesian coordinate system rigidly connected with the cylinder. The plane of flow xOy was limited to a rectangular region of size $(lx, ly) = (100, 100)$. The size was chosen to minimize the effect of external boundaries on the hydrodynamic forces acting on the cylinder. For discretization of the equations we used the finite volume method. The computation scheme was realized on the basis of the OpenFOAM package (Greenshields 2019).

The discretization of the computational domain was carried out using block meshes. The resolution near the cylinder was controlled by the linear mesh grading in the direction normal to the boundary of the cylinder (the characteristic mesh structure in the vicinity of the cylinder is shown in figure 8). The total number of cells N for all calculated cases was $N \approx 3.8 \times 10^5$.

https://doi.org/10.1017/jfm.2020.1180 Published online by Cambridge University Press

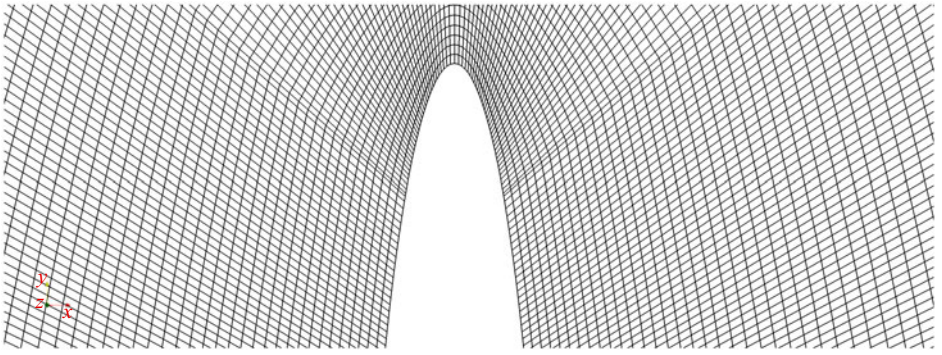


Figure 8. The characteristic mesh structure in the vicinity of the cylinder for $b = 0.1$.

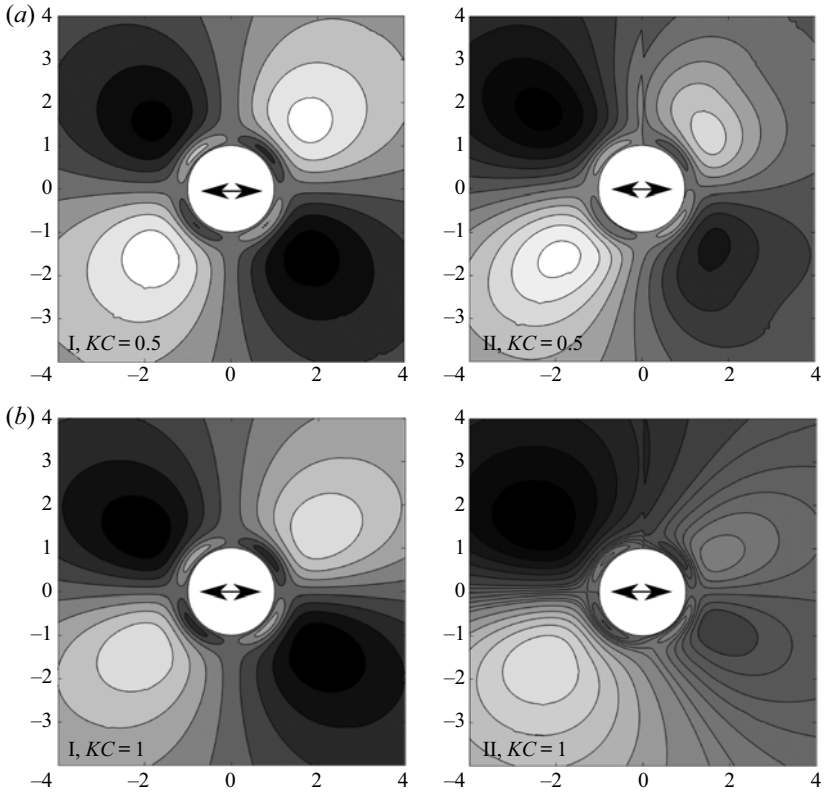


Figure 9. The structure of the steady streaming for harmonic (I) and biharmonic (II) oscillations with various amplitudes KC; $b = 1$, $\beta = 200$, $\alpha = \pi/2$.

Discrete values of the velocity components and the pressure were localized in the cell centres of the computational mesh. The Gauss integral theorem was used to calculate the volume integrals over a finite volume. For the approximation of the pressure gradient, linear interpolation was used. In the diffusion terms the normal velocity gradients on the cell surface were approximated by a second-order symmetric scheme with correction for non-orthogonality (see, e.g. Jasak 1996; Greenshields 2019). For the interpolation of variables in convective terms the hybrid Spalding scheme (Patankar & Spalding 1972;

https://doi.org/10.1017/jfm.2020.1180 Published online by Cambridge University Press

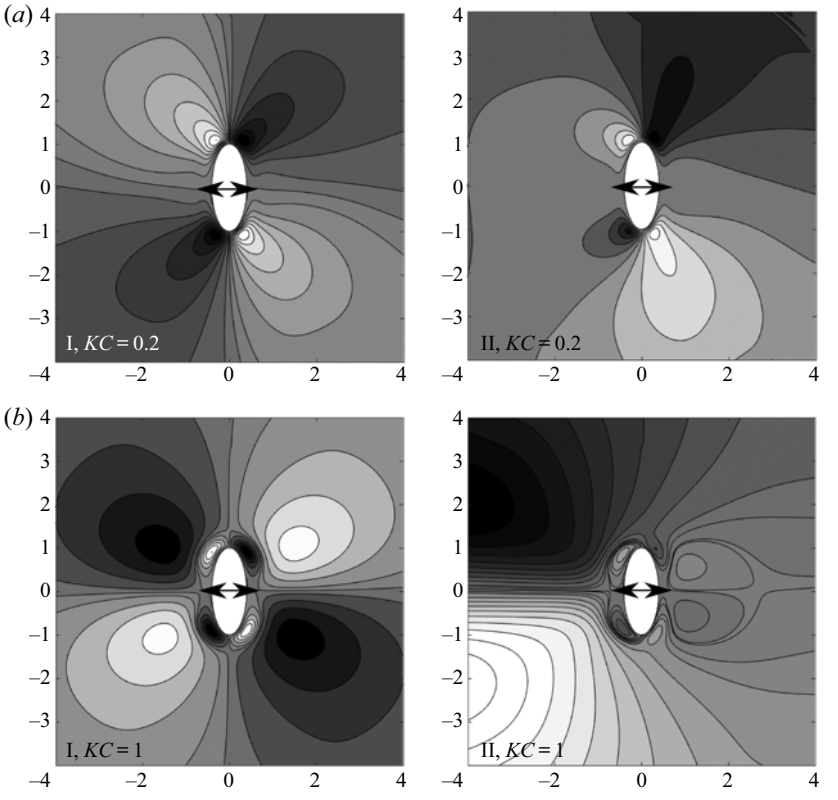


Figure 10. The structure of the steady streaming for harmonic (I) and biharmonic (II) oscillations with various amplitudes KC; $b = 0.4$, $\beta = 200$, $\alpha = \pi/2$.

Spalding 1972) was used. The implicit Euler scheme was used for the discretization of the time derivative. The time step in all calculations was chosen to satisfy the condition that the minimum number of time steps per period must be at least 4000 (for accurate resolution of changes of the hydrodynamic force). The discrete problem was solved using a pressure implicit with splitting of operators (PISO) method (Issa 1986; Ferziger & Perić 1999). The pressure equation was solved by the conjugate gradient method with a generalized geometric-algebraic multigrid preconditioner. The equations for the velocity components were solved using the biconjugate gradient method with a predictor based on incomplete factorization. Domain decomposition techniques and MPI (message passing interface) technology were used for the parallelization of the solution algorithm.

Appendix B. Structure of flows induced by oscillations of an elliptic cylinder

As an auxiliary material, let us present the structural changes of flows under various laws of oscillation in the considered range of parameters. As the asymptotic analysis shows, in the leading unsteady terms, the external flow is potential (see solutions for $\tilde{\Psi}_0$, $\tilde{\Psi}_1$). The vortex structure of the flow in the outer region (at low amplitudes) is mainly determined by the secondary steady streaming. Although secondary streaming at low oscillation amplitudes does not make a significant contribution to the hydrodynamic forces (as was shown in this work, they can only affect the force terms of the order of $O(\varepsilon^3)$

https://doi.org/10.1017/jfm.2020.1180 Published online by Cambridge University Press

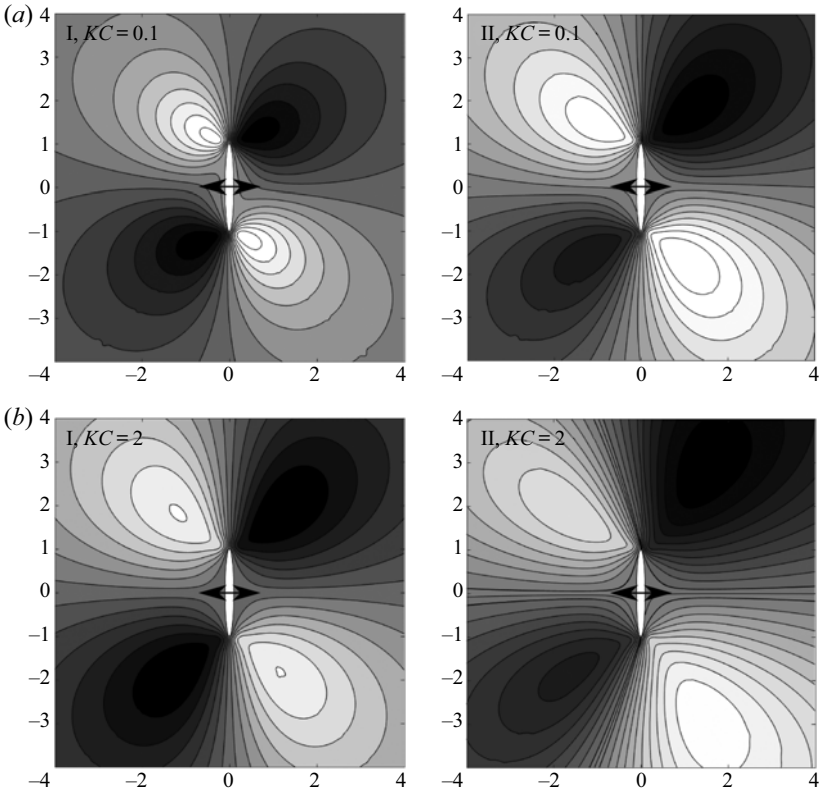


Figure 11. The structure of the steady streaming for harmonic (I) and biharmonic (II) oscillations with various amplitude KC; $b = 0.1$, $\beta = 200$, $\alpha = \pi/2$.

and higher), it is the key mechanism of mass transfer in the region. Next, we present the characteristic flow patterns of the secondary streaming obtained in the framework of numerical simulation for monoharmonic and biharmonic oscillations (determined by (4.13)) for $b = 1, 0.4, 0.1$, $\alpha = \pi/2$, $\beta = 200$.

The structure of the secondary flows around a circular cylinder ($b = 1$) consists of 8 vortex cells: 4 external and 4 internal (see figure 9). For the case of harmonic oscillations, they are symmetrically located relative to the Ox and Oy axes. Such a flow regime was first theoretically described by Schlichting (1932). The asymmetry of the biharmonic law of motion, which determines different speeds of forward and backward motion, leads to symmetry breaking of the flow relative to the Oy axis with an increase of the oscillation amplitude. A noticeable change in the sizes of the external vortex cells located on opposite sides (on the left and on the right) of the cylinder can be observed for $b = 1$ at $KC = 0.5$ (see figure 9).

For the case of $b = 0.4$, the secondary flow at low KC values (see the flow visualization for $KC = 0.2$ in figure 10) consists of 4 vortex cells. Note that such a structure can also be observed around a circular cylinder at small values of β (see, e.g. Nuriev *et al.* 2018). With an increase of KC, the flow transforms into a regime with 8 circulation cells, similar to that observed for $b = 1$. For harmonic oscillations (in both regimes), the cells are located symmetrically about the Ox and Oy axes. For biharmonic oscillations, visible symmetry breaking (relative to the Oy axis) can be observed already at $KC = 0.2$.

https://doi.org/10.1017/jfm.2020.1180 Published online by Cambridge University Press

The flow visualization for the case of $b = 0.1$ is shown in figure 11 for $KC = 0.1$ and $KC = 0.2$. The flow consists of 4 circulation cells. At $KC = 0.1$, the structure of flows induced by harmonic and biharmonic oscillations is practically identical; symmetry with respect to the Ox and Oy axes is observed. The asymmetry of the flow for the case of biharmonic oscillations appears at $KC = 0.2$.

References

Ahsan, S.N. & Aureli, M. 2015 Finite amplitude oscillations of flanged laminas in viscous flows: vortex-structure interactions for hydrodynamic damping control. *J. Fluids Struct.* **59**, 297–315.

An, H., Cheng, L. & Zhao, M. 2015 Two-dimensional and three-dimensional simulations of oscillatory flow around a circular cylinder. *Ocean Engng* **109**, 270–286.

Aureli, M. & Porfiri, M. 2010 Low frequency and large amplitude oscillations of cantilevers in viscous fluids. *Appl. Phys. Lett.* **96** (16), 164102.

Aureli, M., Porfiri, M. & Basaran, M.E. 2012 Nonlinear finite amplitude vibrations of sharp-edged beams in viscous fluids. *J. Sound Vib.* **331** (7), 1624–1654.

Aureli, M., Prince, C., Porfiri, M. & Peterson, S.D. 2010 Energy harvesting from base excitation of ionic polymer metal composites in fluid environments. *Smart Mater. Struct.* **19** (1), 015003.

Bearman, P.W., Graham, J.M.R., Obasaju, E.D. & Drossopoulos, G.M. 1984 The influence of corner radius on the forces experienced by cylindrical bluff bodies in oscillatory flow. *Appl. Ocean Res.* **6** (2), 83–89.

Bearman, P.W., Downie, M.J., Graham, J.M.R. & Obasaju, E.D. 1985*a* Forces on cylinders in viscous oscillatory flow at low Keulegan–Carpenter numbers. *J. Fluid Mech.* **154** (1), 337–356.

Bearman, P.W., Downie, M.J., Graham, J.M.R. & Obasaju, E.D. 1985*b* Forces on cylinders in viscous oscillatory flow at low Keulegan–Carpenter numbers. *J. Fluid Mech.* **154**, 337–356.

Bidkar, R.A., Kimber, M., Raman, A., Bajaj, A.K. & Garimella, S.V. 2009 Nonlinear aerodynamic damping of sharp-edged flexible beams oscillating at low Keulegan–Carpenter numbers. *J. Fluid Mech.* **634**, 269–289.

Brumley, D.R., Willcox, M. & Sader, J.E. 2010 Oscillation of cylinders of rectangular cross section immersed in fluid. *Phys. Fluids* **22** (5), 052001.

Daoud, S., Nehari, D., Aichouni, M. & Nehari, T. 2015 Numerical simulations of an oscillating flow past an elliptic cylinder. *Trans. ASME: J. Offshore Mech. Arctic Engng* **138** (1), 011802.

Davidson, B.J. & Riley, N. 1972 Jets induced by oscillatory motion. *J. Fluid Mech.* **53** (2), 287–303.

Dehdari Ebrahimi, N., Eldredge, J.D. & Ju, Y.S. 2019 Wake vortex regimes of a pitching cantilever plate in quiescent air and their correlation with mean flow generation. *J. Fluids Struct.* **84**, 408–420.

Duck, P.W. & Smith, F.T. 1979 Steady streaming induced between oscillating cylinders. *J. Fluid Mech.* **91** (1), 93–110.

Egorov, A.G., Kamalutdinov, A.M. & Nuriev, A.N. 2018 Evaluation of aerodynamic forces acting on oscillating cantilever beams based on the study of the damped flexural vibration of aluminium test samples. *J. Sound Vib.* **421**, 334–347.

Egorov, A.G., Kamalutdinov, A.M., Nuriev, A.N. & Paimushin, V.N. 2014 Theoretical-experimental method for determining the parameters of damping based on the study of damped flexural vibrations of test specimens 2. Aerodynamic component of damping. *Mech. Compos. Mater.* **50** (3), 267–278.

Egorov, A.G., Kamalutdinov, A.M., Nuriev, A.N. & Paimushin, V.N. 2017 Experimental determination of damping of plate vibrations in a viscous fluid. *Dokl. Phys.* **62** (5), 257–261.

Erturk, A. & Inman, D.J. 2011 *Piezoelectric Energy Harvesting*. Wiley.

Ferziger, J.H. & Perić, M. 1999 *Computational Methods for Fluid Dynamics*, 2nd edn. Springer.

Gallardo, J.P., Andersson, H.I. & Pettersen, B. 2016 Three-dimensional instabilities in oscillatory flow past elliptic cylinders. *J. Fluid Mech.* **798**, 371–397.

Graham, J.M.R. & Djahansouzi, B. 1989 Hydrodynamic damping of structural elements. In *Proceedings of the Eighth International Conference on Offshore Mechanics and Arctic Engineering*, vol. II, pp. 289–293. American Society of Mechanical Engineers.

Graham, J.M.R. 1980 The forces on sharp-edged cylinders in oscillatory flow at low Keulegan–Carpenter numbers. *J. Fluid Mech.* **97** (02), 331–346.

Greenshields, C. 2019 OpenFOAM v7 User Guide.

Haddon, E.W. & Riley, N. 1979 The steady streaming induced between oscillating circular cylinders. *Q. J. Mech. Appl. Maths* **32** (2), 265–282.

https://doi.org/10.1017/jfm.2020.1180 Published online by Cambridge University Press

HOLTSMARK, J., JOHNSEN, I., SIKKELAND, T. & SKAVLEM, S. 1954 Boundary layer flow near a cylindrical obstacle in an oscillating, incompressible fluid. *J. Acoust. Soc. Am.* **26** (1), 26–39.

ISSA, R.I. 1986 Solution of the implicitly discretised fluid flow equations by operator-splitting. *J. Comput. Phys.* **62** (1), 40–65.

JASAK, H. 1996 Error analysis and estimation for the finite volume method with applications to fluid flows. Phd thesis, Department of Mechanical Engineering Imperial College of Science, Technology and Medicine.

JUSTESEN, P. 1991 A numerical study of oscillating flow around a circular cylinder. *J. Fluid Mech.* **222**, 157–196.

KANWAL, R.P. 1955 Vibrations of an elliptic cylinder and a flat plate in a viscous fluid. *Z. Angew. Math. Mech.* **35** (1–2), 17–22.

KEULEGAN, G.H. & CARPENTER, L.H. 1958 Forces on cylinders and plates in an oscillating fluid. *J. Res. Natl Bur. Stand.* **60** (5), 423–440.

KIM, S.K. & TROESCH, A.W. 1989 Streaming flows generated by high-frequency small-amplitude oscillations of arbitrarily shaped cylinders. *Phys. Fluids* A **1** (6), 975–985.

KOPMAN, V. & PORFIRI, M. 2013 Design, modeling, and characterization of a miniature robotic fish for research and education in biomimetics and bioinspiration. *IEEE/ASME Trans. Mechatron.* **18** (2), 471–483.

LANDAU, L.D. & LIFSHITZ, E.M. 1987 *Fluid Mechanics: Volume 6*. Elsevier Science.

MILNE-THOMSON, L.M. 1960 *Theoretical Hydrodynamics by L.M. Milne-Thomson*. Macmillan.

MORISON, J.R., JOHNSON, J.W. & SCHAAF, S.A. 1950 The force exerted by surface waves on piles. *J. Petrol. Technol.* **2** (05), 149–154.

NOCA, F., SHIELS, D. & JEON, D. 1999 A comparison of methods for evaluating time-dependent fluid dynamic forces on bodies, using only velocity fields and their derivatives. *J. Fluids Struct.* **13** (5), 551–578.

NURIEV, A.N. & EGOROV, A.G. 2019 Asymptotic investigation of hydrodynamic forces acting on an oscillating cylinder at finite streaming Reynolds numbers. *Lobachevskii J. Math.* **40**, 794–801.

NURIEV, A.N., EGOROV, A.G. & ZAITSEVA, O.N. 2018 Numerical analysis of secondary flows around an oscillating cylinder. *J. Appl. Mech. Tech. Phys.* **59** (3), 451–459.

NURIEV, A.N., KAMALUTDINOV, A.M. & EGOROV, A.G. 2019 A numerical investigation of fluid flows induced by the oscillations of thin plates and evaluation of the associated hydrodynamic forces. *J. Fluid Mech.* **874**, 1057–1095.

OH, M.H., SEO, J., KIM, Y.-H. & CHOI, M. 2019 Endwall effects on 3d flow around a piezoelectric fan. *Eur. J. Mech.* B/*Fluids* **75**, 339–351.

PAIMUSHIN, V.N., FIRSOV, V.A. & SHISHKIN, V.M. 2019 Identification of the dynamic elasticity characteristics and damping properties of the ot-4 titanium alloy based on study of damping flexural vibrations of the test specimens. *J. Mach. Manuf. Reliab.* **48**, 119–129.

PATANKAR, S.V. & SPALDING, D.B. 1972 A calculation procedure for heat, mass and momentum transfer in three-dimensional parabolic flows. *Intl J Heat Mass Transfer* **15** (10), 1787–1806.

PAYAM, A.F., TREWBY, W. & VOÏTCHOVSKY, K. 2017 Simultaneous viscosity and density measurement of small volumes of liquids using a vibrating microcantilever. *Analyst* **142** (9), 1492–1498.

PHAN, C.N., AURELI, M. & PORFIRI, M. 2013 Finite amplitude vibrations of cantilevers of rectangular cross sections in viscous fluids. *J. Fluids Struct.* **40**, 52–69.

RAY, M. 1936 Vibration of an infinite elliptic cylinder in a viscous liquid. *Z. Angew. Math. Mech.* **16** (2), 99–108.

RILEY, N. 1967 Oscillatory viscous flows, review and extension. *IMA J. Appl. Maths* **3** (4), 419–434.

RILEY, N. 1975 The steady streaming induced by a vibrating cylinder. *J. Fluid Mech.* **68**, 801–812.

SADER, J.E. 1998 Frequency response of cantilever beams immersed in viscous fluids with applications to the atomic force microscope. *J. Appl. Phys.* **84** (1), 64.

SARPKAYA, T. 1986 Forces on a circular cylinder in viscous oscillatory flow at low Keulegan–Carpenter numbers. *J. Fluid Mech.* **165**, 61–71.

SCHERER, M.P., FRANK, G. & GUMMER, A.W. 2000 Experimental determination of the mechanical impedance of atomic force microscopy cantilevers in fluids up to 70 KHz. *J. Appl. Phys.* **88** (5), 2912–2920.

SCHLICHTING, H. 1932 Berechnung ebener periodischer grenzschichtströmungen. *Phys. Zeit.* **33**, 327–335.

SHIH, C.C. & BUCHANAN, H.J. 1971 The drag on oscillating flat plates in liquids at low Reynolds numbers. *J. Fluid Mech.* **48** (2), 229–239.

SHINTAKE, J., CACUCCIOLO, V., SHEA, H. & FLOREANO, D. 2018 Soft biomimetic fish robot made of dielectric elastomer actuators. *Soft Robot.* **5** (4), 466–474.

SINGH, S. 1979 Forces on bodies in oscillatory flow. PhD thesis, University of London.

SPALDING, D.B. 1972 A novel finite difference formulation for differential expressions involving both first and second derivatives. *Intl J. Numer. Meth. Engng* **4** (4), 551–559.

https://doi.org/10.1017/jfm.2020.1180 Published online by Cambridge University Press

STOKES, G.G. 1851 On the effect of the internal friction of fluids on the motion of pendulums. *Trans. Camb. Phil. Soc.* **9**, 8–106.

STUART, J. 1966 Double boundary layers in oscillatory viscous flow. *J. Fluid Mech.* **24**, 673–687.

TUCK, E.O. 1969 Calculation of unsteady flows due to small motions of cylinders in a viscous fluid. *J. Engng Maths* **3** (1), 29–44.

WANG, C.-Y. 1968 On high-frequency oscillatory viscous flows. *J. Fluid Mech.* **32** (01), 55.

WYBROW, M.F., YAN, B. & RILEY, N. 1996 Oscillatory flow over a circular cylinder close to a plane boundary. *Fluid Dyn. Res.* **18** (5), 269–288.

YEH, P.D. & ALEXEEV, A. 2014 Free swimming of an elastic plate plunging at low Reynolds number. *Phys. Fluids* **26** (5), 053604.

YEH, P.D., DEMIRER, E. & ALEXEEV, A. 2019 Turning strategies for plunging elastic plate propulsor. *Phys. Rev. Fluids* **4**, 064101.

YOUSSEF, F.A. 1999 High frequency oscillating viscous flow over elliptic cylinder at incidence. *Acta Mech.* **133**, 161–174.

https://doi.org/10.1017/jfm.2020.1180 Published online by Cambridge University Press